THE JOURNAL OF PHYSICAL CHEMISTRY A

Article

pubs.acs.org/JPCA

Hydration Enthalpies of $Ba^{2+}(H_2O)_x$, $x = 1-8$: A Threshold Collision-Induced Dissociation and Computational Investigation

Oscar W. Wheeler, Damon R. Carl,[†] Theresa E. Hofstetter,[‡] and P. B. Armentrout*

Department of Chemistry, University of Utah, 315 South 1400 East, Room 2020, Salt Lake City, Utah 84112, United States

Supporting Information

ABSTRACT: The sequential bond dissociation energies (BDEs) of $Ba^{2+}(H_2O)_x$ complexes, where $x = 1-8$, are determined using threshold collision-induced dissociation (TCID) in a guided ion beam tandem mass spectrometer. The electrospray ionization source generates complexes ranging in size from $x = 6$ to $x = 8$ with smaller complexes, $x = 1-5$, formed by an in-source fragmentation technique. The only products observed result from sequential loss of water ligands. Charge separation, a process in which both hydrated singly charged barium hydroxide and hydronium ion are formed, was not observed except for $Ba^{2+}(H_2O)_3$ yielding $BaOH^+ + H_5O_2^+$. Modeling of the kinetic energy-dependent cross sections, taking into account the number of collisions, energy distributions, and lifetime effects for both primary and secondary water loss, provides 0 K BDEs. Experimental thermochemistry for the $x = 1-3$ complexes is obtained here for the first time. Hydration enthalpies and reaction coordinate pathways for charge separation are also examined computationally at several levels of theory. Our experimental and computational work are in excellent agreement in the $x = 1-6$ range. The present experimental values and theoretical calculations are also in reasonable agreement with the available literature values for experiment, $x = 4-8$, and theory, $x = 1-6$. Of the numerous calculations performed in the current study, B3LYP/DHF/def2-TZVPP calculations including counterpoise corrections reproduce our experimental values the best, although MP2(full)/DHF/def2-TZVPP//B3LYP/DHF/def2-TZVPP results are comparable.

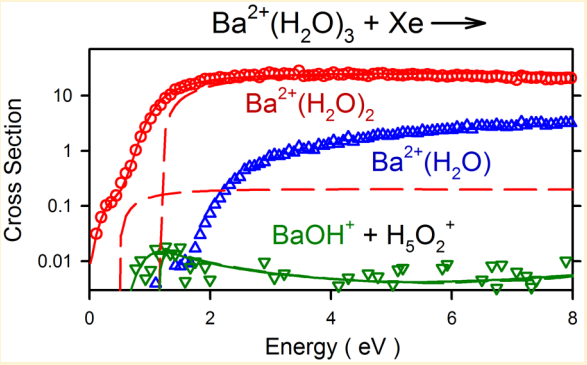

1. INTRODUCTION

The presence of barium ions in aqueous solutions occurs both naturally and from anthropogenic release. Ba^{2+} ions are known to have some toxic effects in humans in small concentrations, with a maximum contaminant level of 2.0 mg/L.[1] The soluble Ba^{2+} ions can act as a competitive antagonist to K^+ channels, leading to irregular muscle contraction. The disruption in regulated muscle contraction can specifically affect heart function, with increased blood pressure a possible side effect.[1,2] Some insight into these phenomena can potentially be provided by fundamental examinations of how barium dications interact with their environment and in particular water. The thermodynamics associated with water binding to Ba^{2+} may be particularly useful in understanding the driving forces for delivery of these ions to biologically active sites. The closed shell nature of the barium dication makes it an attractive system for study, with both experimental and theoretical work previously published in the literature. High-pressure mass spectrometry (HPMS) was used by Kebarle and co-workers to examine $Ba^{2+}(H_2O)_x$ complexes ranging from $x = 5$ to $x = 14$,[3−6] whereas the Williams group utilized blackbody infrared radiative dissociation (BIRD) to study $x = 4-7$.[7] More recent work by Williams and co-workers examined the coordination number (CN) of hydrated alkaline earth metals with infrared photodissociation action spectroscopy.[8] To date, no experimental thermochemistry of the smallest complexes, $x = 1-3$, has been obtained because the smaller $Ba^{2+}(H_2O)_x$ complexes are too strongly bound to observe appreciable dissociation over the temperature ranges available to HPMS[3−6] and BIRD.[7]

Theoretical studies of hydrated barium complexes include several reports, but are generally limited to complexes with $x < 7$. Kaupp and Schleyer[9,10] calculated binding energies for the $x = 1$ and 2 water complexes at Hartree−Fock (HF) and second-order Möller−Plesset perturbation (MP2) levels of theory (fourth-order MP4 for $x = 1$). Glendening and Feller[11] found binding energies for the $x = 1-6$ water complexes using the restricted Hartree−Fock (RHF) and MP2 levels of theory. Cao and Wang studied a larger range of complexes, $x = 1-30$, utilizing a "fast hybrid global optimization algorithm" with the TIP4P model for water (a parametrized representation of the water molecule useful for the larger clusters).[12] Beyer, Williams, and Bondybey[13] used B3LYP/SECP/6-311+(3df,2pd) to examine the charge separation reaction in which $Ba^{2+}(H_2O)_2$ dissociates to $BaOH^+ + H_3O^+$. (B3LYP combines the Becke three-parameter hybrid functional with the correlation functional of Lee, Yang, and Parr.[14,15]) A more comprehensive

Received: February 3, 2015
Revised: March 26, 2015
Published: March 30, 2015

DOI: 10.1021/acs.jpca.5b01087
J. Phys. Chem. A 2015, 119, 3800−3815

examination of the charge separation processes for $x = 2-6$ was performed by Miliordos and Xantheas utilizing the MP2 level of theory with an ECP46MDF-f (ADZ) or an ECP46MDF (ATZ) relativistic pseudopotential coupled with the aug-cc-pVDZ and aug-cc-pVTZ basis sets, respectively, for oxygen and hydrogen atoms.[16] These authors considered multiple pathways including those forming H_3O^+ and $H_5O_2^+$.

A number of hydrated dications have been investigated previously in our laboratory: the alkaline earth metals (group 2), Mg^{2+}, Ca^{2+}, and Sr^{2+};[17−20] group 12 elements, Zn^{2+} and Cd^{2+};[21−24] and open-shell transition metals, Fe^{2+} and Cu^{2+}.[25,26] Here we extend this work on alkaline earth metals to the hydration of Ba^{2+}, the next heavier group 2 metal dication, and examine $Ba^{2+}(H_2O)_x$ complexes ranging in size from $x = 1$ to $x = 8$ both experimentally and computationally. These complexes are generated under thermalized conditions by utilizing an electrospray ionization (ESI) source and in-source fragmentation technique.[27,28] A guided ion beam tandem mass spectrometer is then utilized to examine the collision-induced dissociation behavior of the complexes as a function of kinetic energy. The results are interpreted to obtain experimental hydration energies of the $Ba^{2+}(H_2O)_x$ complexes. In addition, we undertake an examination of the theoretical binding energies and geometries that is more thorough than those found in the literature. These computations provide the molecular parameters used in the analysis of the data, and comparison of the theoretical and experimental bond energies permit the structures of the experimentally investigated complexes to be identified. Multiple levels of theory with a number of different basis sets are used to find low-energy conformations for the $Ba^{2+}(H_2O)_x$ complexes, $x = 1-8$.

Although collision-induced dissociation of $M^{2+}(H_2O)_x$ complexes generally leads to loss of water ligands, complexes of specific sizes are observed to undergo a charge separation process in which one or more inner shell water molecules is promoted to outer shells followed by transfer of a proton, forming $MOH^+(H_2O)_y + H^+(H_2O)_{x-y-1}$.[17−26,29] Similar processes have been observed in the photodissociation of $M^{3+}(H_2O)_x$ complexes.[30] The present study includes both an experimental and theoretical examination of the hydrated barium dication complexes undergoing dissociation via the charge separation process. The $M^{2+}(H_2O)_x$ complex size where charge separation becomes energetically favored compared to single water loss is considered the critical size (x_c).[22] Previous alkaline earth metal studies[17,19,20] found x_c is 3 ($y = 1$) or 4 ($y = 2$) for Mg^{2+} and 2 ($y = 0$) for both Ca^{2+} and Sr^{2+}. This suggests that charge separation, if energetically favorable, might be observed for only the $Ba^{2+}(H_2O)_2$ complex. In previous work done using an ESI source and a triple-quadrupole mass spectrometer, $BaOH^+$ was observed as a minor product when examining the $Ba^{2+}(H_2O)_6$ + Ar dissociation, but neither the immediate precursor nor the accompanying $H^+(H_2O)_z$ species could be identified.[29] Another study performed using a multisector selected-ion flow tube tandem mass spectrometer with an electrospray source found no evidence for charge separation products with barium at room temperature.[31] It is possible that the $BaOH^+$ product detected in this work arises from the presence of low-lying isomers within the reactant beam.

2. EXPERIMENTAL AND COMPUTATIONAL METHODS

2.1. General Experimental Procedures. Threshold collision-induced dissociation (TCID) cross sections of $Ba^{2+}(H_2O)_x$ with Xe are measured using a guided ion beam tandem mass spectrometer, described in detail elsewhere.[32,33] Briefly, an ESI source[20] is used to generate hydrated barium complexes by using a 10^{-4} M solution of $BaCl_2$ dissolved in high-performance liquid chromatography water that is advanced at a rate of 0.05 mL/h through a 35 gauge stainless steel needle. The needle has an applied voltage of ∼2 kV relative to the orifice of a heated capillary (80 °C) used to introduce the ions into the vacuum system. The capillary is followed by an 88-plate radio frequency (rf) ion funnel that collects and focuses the ions.[28,34−36] At the end of the funnel, the ions are injected into an rf-only hexapole where they undergo multiple collisions (>10^4) with ambient gas allowing thermalization to occur. The internal energies of the reactants can be characterized with a Maxwell−Boltzmann distribution at 300 K, as previously shown.[20,27,28]

While in the hexapole, the ions transfer to a lower-pressure vacuum chamber where they are extracted and focused into a magnetic momentum analyzer for mass selection. Complexes are then decelerated to a well-defined kinetic energy and enter the rf octopole ion guide where radial trapping occurs.[32,37,38] While in the octopole, reactants pass through a collision cell containing xenon gas at pressures sufficiently low that single-collision conditions prevail. Xenon is used for efficient translational to internal energy transfer during collisions, as detailed elsewhere.[39,40] After the octopole, reactant and product ions are focused into a quadrupole mass filter for mass analysis. Ion intensities are measured using a Daly detector[41] and standard pulse counting techniques.

For larger $Ba^{2+}(H_2O)_x$ complexes, $x = 6-8$, the ESI source generates sufficient intensity for TCID studies. For smaller complexes, $x = 1-5$, an in-source fragmentation technique is used to generate higher intensities of the reactant ions. As previously described,[27] negative voltages on dc electrodes placed between the hexapole rods induce fragmentation of the initial ion distribution (probably by rf heating). When the dc voltage is increased, increasingly smaller complexes are generated; however, previous work[27] has shown that if the voltage placed on the dc electrodes is too large, complete thermalization of the ions may not occur, resulting in excited conformers. To avoid this, the evolution of the experimental thresholds are monitored as the voltage applied to the electrodes is increased and only results corresponding to the lowest-energy $Ba^{2+}(H_2O)_x$ conformers, which should correspond to thermalized 300 K complexes, are analyzed below.

Conversion of ion intensities to absolute reaction cross sections has been previously described,[32] with uncertainties estimated at ±20%. In the octopole region, ions are accelerated by V_{Lab}, the voltage difference between the dc bias on the source hexapole and the octopole. Because the complexes are doubly charged, their kinetic energy is twice that of the applied voltage, $E_{Lab} = 2 \times V_{Lab}$. Laboratory frame energies (E_{Lab}) are converted to the center-of-mass (CM) frame using the formula $E_{CM} = E_{Lab} \times m/(m + M)$, where m represents the mass of Xe and M that of the reactant ion. A retarding potential on the octopole is used to determine the kinetic energy zero and distribution for the ion beam,[32] which has a full width at half-maximum of 0.10−0.15 eV. The uncertainty in the absolute energy scale is 0.05 eV (V_{Lab}). All energies reported below are in the CM frame.

2.2. Thermochemical Analysis. To model the kinetic energy-dependent cross sections for single water molecule loss from reactant $Ba^{2+}(H_2O)_x$ complexes, a modified empirical

DOI: 10.1021/acs.jpca.5b01087
J. Phys. Chem. A 2015, 119, 3800−3815

threshold model is utilized. To ensure accurate thermodynamic data when modeling, a number of effects are considered, including multiple collisions, lifetime effects, and energy distributions. Single-collision conditions are maintained by obtaining cross sections at multiple pressures of Xe, in this case ~0.2, 0.1, and 0.05 mTorr, and extrapolating to zero pressure.[42] The increasing complexity of larger $Ba^{2+}(H_2O)_x$ ions can lead to a failure to dissociate within the time scale of the experiment, $\tau \approx 5 \times 10^{-4}$ s. To account for this effect, Rice–Ramsperger–Kassel–Marcus (RRKM) statistical theory[43−45] is incorporated into the empirical threshold model, as discussed elsewhere[46] and shown in eq 1.

$$\sigma_j(E) = \left(\frac{n\sigma_{0,j}}{E}\right)\Sigma_i g_i \int_{E_{0,j}-E_i}^{E} (k_j/k_{tot})P_{D1}(E-\varepsilon)^{n-1}\,d\varepsilon \quad (1)$$

Here, $\sigma_{0,j}$ is an energy-independent scaling factor for channel j and E represents the reactants' relative translational energy. $E_{0,j}$ is the reaction threshold for channel j at 0 K, and n is an adjustable fitting parameter that describes the efficiency of energy transfer during collision.[33] The summation is over the rovibrational states of the reactant ions having excitation energies, E_i, and populations, g_i, where $\sum g_i = 1$. Vibrational frequencies and rotational constants are taken from quantum chemical calculations discussed below. The internal energy distribution is evaluated using the Beyer–Swinehart–Stein–Rabinovich algorithm.[44,47−49] Relative populations, g_i, are computed for a Maxwell–Boltzmann distribution at 300 K. Energy deposited into the ion upon collision with xenon is represented by ε such that the internal energy of the energized molecule (EM) is $E^* = \varepsilon + E_i$ and $P_{D1} = 1 - \exp[-k_{tot}(E^*)\tau]$ is the dissociation probability, where the RRKM unimolecular dissociation rate coefficient for channel j is given by eq 2.

$$k_j(E^*) = sN_{vr}^{\dagger}(E^* - E_{0,j})/h\rho_{vr}(E^*) \quad (2)$$

Here, s is the reaction degeneracy calculated from the ratio of the rotational symmetry numbers of reactants and products, $N_{vr}^{\dagger}(E^*-E_{0,j})$ the sum of rovibrational states for the transition state (TS) of channel j at an energy $E^*-E_{0,j}$ above the threshold, ρ_{vr} the density of rovibrational states for the EM at E^*, and $k_{tot} = \Sigma k_j$. The accuracy of eq 1 for estimating kinetic shifts has been supported in a number of previous studies.[17−26]

A sequential dissociation model (for brevity, referred to as "sequential model(ing)") described elsewhere[50] is used to analyze data for the loss of two water molecules from the reactant $Ba^{2+}(H_2O)_x$ complexes. In the sequential model, the energy available to the primary products, $E_1^{\dagger} = E^*-E_0$, can be partitioned into translational energy (T_1), internal energy of the product ligand (E_L), and internal energy of the product ion undergoing further dissociation (E_2^*), as shown in eq 3.

$$E_1^{\dagger} = T_1 + E_L + E_2^* \quad (3)$$

With the partitioning assumed to behave statistically,[50] the dissociation probability of the products is $P_{D2} = 1 - \exp[-k_2(E_2^*)\tau]$. Thus, the cross section for the secondary product ion is predicted by multiplying the primary cross section from eq 1 with P_{D2}.

To calculate the RRKM unimolecular rate coefficients of eq 2, rovibrational states for the EM and TS are needed.[43−45] Results of quantum chemical calculations of the reactant ion described below are used for the molecular parameters of the EM. For loss of water, a loose phase-space limit (PSL) TS with no reverse activation barrier is assumed because this process corresponds to a heterolytic bond cleavage.[51] Transitional modes of the dissociating $Ba^{2+}(H_2O)_x$ complexes are treated as rotors and calculated from the rotational constants of the $Ba^{2+}(H_2O)_{x-1}$ and H_2O products. The TS is assumed to be located at the centrifugal barrier for dissociation to products and is calculated using a variational approach outlined elsewhere.[46] The two-dimensional (2D) external rotations are treated adiabatically, but include centrifugal effects,[52] and are calculated as a statistical distribution with an explicit summation over the possible values of the rotational quantum number.[46] For charge separation channels, the TS is tight with molecular parameters taken directly from the calculations described below.

The model cross sections of eq 1 and the sequential model are convoluted over the kinetic energy distributions of the $Ba^{2+}(H_2O)_x$ complex (experimentally determined as outlined above) and Xe gas (Maxwell–Boltzmann distribution at 300 K) before comparison to experimental cross sections.[32] The parameters σ_0, n, and $E_{0,j}$ are optimized with a nonlinear least-squares fitting procedure. Because there should be no activation barriers beyond the endothermicity of the reaction for loss of water,[51] $E_{0,j}$ represents the binding energy of H_2O to the $Ba^{2+}(H_2O)_{x-1}$ complex at 0 K. Uncertainties in the modeling parameters are found by scaling vibrational frequencies up and down by 10%, varying the best fit n value up and down by 0.1, and scaling the average experimental lifetime available for dissociation up and down by a factor of 2. The absolute uncertainty in the energy scale (0.05 eV_{Lab}) is also included in E_0 uncertainties.

2.3. Computational Details. All quantum chemical calculations in the current work were performed using Gaussian09[53] and the workstations of the Center for High Performance Computing (CHPC) at the University of Utah. Geometries previously published for $Ca^{2+}(H_2O)_x$ complexes[19] served as a starting point for many $Ba^{2+}(H_2O)_x$ complexes. Initial geometry optimizations of the $Ba^{2+}(H_2O)_x$ complexes were done at a B3LYP/SDD/def2-TZVP[14,15] level of theory. The def2-TZVP basis set[54] is a balanced basis set of triple-ζ quality plus polarization functions, which is used for all the atoms along with the 1991 quasirelativistic Stuttgart–Dresden (SDD) small core effective core potential (ECP) for Ba^{2+}, also called ECP46MWB.[9] For comparison, B3LYP geometry optimizations were also performed with two other basis sets, SDD/6-311+G(d,p) and HW*/6-311+G(d,p), which use the 6-311+G(d,p) basis set for O and H atoms. The former uses the SDD ECP (ECP46MWB) and basis set for Ba and the latter the Hay–Wadt[55] (HW) ECP and basis set for Ba with an added polarization function (as indicated by *).[11] Vibrational frequencies and rotational constants were calculated with all three basis sets and the B3LYP functional. Only minor differences were found between the lowest-energy structures found with the different basis sets; hence, the current work focuses on the def2-TZVP results as these have been found to accurately predict vibrational frequencies of barium complexes in other studies.[56] B3LYP is used because this density functional approach has proven successful in our previous studies of metal cation hydration.

Vibrational frequencies were scaled by 0.989 and used to calculate zero point energies (ZPEs) and thermal corrections.[57] Using the B3LYP geometries from the three different basis sets, single-point energies were calculated with the B3LYP, B3P86, and M06 functionals along with MP2(full) perturbation theory (where "full" indicates all electrons outside the ECP are

DOI: 10.1021/acs.jpca.5b01087
J. Phys. Chem. A 2015, 119, 3800−3815

included in the correlation calculation) using slightly larger HW*/6-311+G(2d,2p), SDD/6-311+G(2d,2p), and SDD/def2-TZVPP basis sets. The B3LYP, B3P86, M06, and MP2(full) levels of theory are used for consistency with previous studies on hydration of the alkaline earth metal dications.[17−20] The M06 level is included because this functional is designed to better model noncovalent interactions, such as the hydrogen bonds found in a second hydration shell around Ba^{2+}.[58] A larger basis set for the hydrated complexes, in relation to previous theoretical work,[10,11] is used to ensure accurate thermodynamic information. Basis set superposition error (BSSE) corrections were calculated using the full counterpoise method.[59,60] Counterpoise corrections for the MP2(full) values, 3−11 kJ/mol, are higher than those for the density functional approaches, which were in the 1−6 kJ/mol range. In both instances, these corrections improve agreement with experimentally derived bond dissociation energies.

The role of basis set size on both geometry and single-point energy was investigated as well. B3LYP geometry optimizations were also performed using the slightly larger def2-TZVPP for O and H atoms and either the def2-TZVPP or DHF-TZVPP (DHF)[61] basis set for Ba^{2+}. The larger DHF basis set utilizes an ECP46MDF relativistic pseudopotential with additional Gaussian functions, [6s5p3d2f1g].[61] These geometries were then used in single-point energy calculations at the B3P86, M06, and MP2(full) levels of theory with each corresponding basis set. Here, counterpoise corrections are similar to those for the smaller basis sets, whereas MP2(full) corrections were somewhat larger for larger complexes.

Results for all zero-point energy corrected (0 K) bond enthalpies, with and without counterpoise corrections, generated from the different levels of theory and corresponding basis sets can be found in Table S1 of the Supporting Information. All bond energies calculated using the aforementioned levels of theory and basis sets are similar; hence, the discussion below will emphasize results obtained using the B3LYP/SDD/def2-TZVP optimized geometries for modeling of the experimental results and the B3LYP and MP2(full)/DHF/def2-TZVPP single-point energies for theoretical BDEs.

Additional geometry optimizations and single-point energy calculations for $Ba^{2+}(H_2O)_x$ were performed with dispersion corrections[62,63] at the B3LYP-GD3BJ/SDD/def2-TZVPP (x = 1−8) and B3LYP-GD3BJ/DHF/def-2TZVPP (x = 1−6) levels followed also by single-point calculations using M06-GD3/SDD/def2-TZVPP and M06-GD3/DHF/def2-TZVPP, respectively. Dispersion corrections increase the B3LYP counterpoise corrected bond energies by 2−10 kJ/mol for the SDD/def2-TZVPP and DHF/def2-TZVPP basis sets, except for the x = 2 structure using the latter basis set. This species has a geometry that is slightly different than that of the nondispersion corrected structure, which leads to a bond energy that is lower by 1 kJ/mol for the dispersion-corrected bond energy. The M06-GD3 bond energies (SDD/def2-TZVPP and DHF/def2-TZVPP basis sets) differ from those without dispersion corrections by −4 to 3 kJ/mol. For both B3LYP and M06, such corrections worsen the agreement between experiment and theory (see Table S1 of the Supporting Information); hence, these results are not included in the discussion below. The dispersion corrections do not change the relative energies of the x = 7 isomers but do lower the energy of the (8,0) complex relative to (7,1) and (6,2), see Table S2 of the Supporting Information. Indeed, (8,0) becomes the predicted ground state at the M06-GD3/SDD/def2-TZVPP level of theory.

3. RESULTS

3.1. Cross Sections for Threshold Collision-Induced Dissociation. TCID cross sections with Xe for $Ba^{2+}(H_2O)_x$, where x = 1−8, were obtained. Those for x = 1, 2, 5, and 8 are shown in Figure 1, and those for all complexes can be found in the Supporting Information, Figure S1. In all cases, the dominant reaction path is the loss of a single water molecule, reaction 4.

$$Ba^{2+}(H_2O)_x + Xe \rightarrow Ba^{2+}(H_2O)_{x-1} + H_2O + Xe \quad (4)$$

As the kinetic energy increases, additional water molecules are sequentially lost and can eventually form the bare Ba^{2+} ion. In all cases, the total cross section rises sharply with energy with thresholds that gradually decrease as x increases. At higher energies, the total cross section plateaus to a nearly constant magnitude with values that gradually increase with the size of the complex. The magnitudes of these cross sections are similar to those found for the other alkaline earth metals.[17−20]

Charge separation products, $BaOH^+(H_2O)_y$ and $H^+(H_2O)_{x-y-1}$, were specifically looked for with all x = 2−8 complexes. Only the $Ba^{2+}(H_2O)_3$ system was found to yield any such products, specifically $BaOH^+$, and this only under conditions where the magnitude of the parent complexes was optimized, potentially leading to internal excitation, as discussed further below. The intensity of the $BaOH^+$ complex was only slightly larger than that of our background noise. Our observation is consistent with the formation of this product in reaction 5

$$Ba^{2+}(H_2O)_3 + Xe \rightarrow BaOH^+ + H^+(H_2O)_2 + Xe \quad (5)$$

otherwise $BaOH^+(H_2O)$ should have been observed. The failure to observe the $H^+(H_2O)_2$ product of reaction 5 can be attributed to the substantial kinetic energy release associated with the charge separation reaction, a result of the Coulomb repulsion between the two products. In such cases, the lighter mass product has a much larger velocity, making its collection more difficult, as confirmed by previous studies.[17,19,20,25]

3.2. Theoretical Geometries for $Ba^{2+}(H_2O)_x$ Complexes, x = 1−4. A full exploration of various isomers of these complexes was conducted at the B3LYP/SDD/def2-TZVP level of theory. The most stable geometries of the small complexes found here are similar to those of the previously studied alkaline earth metal dication systems[17,19,20] and are pictured in Figure 2. For structures having the lowest relative energies (which for convenience we refer to as ground structures, GSs below) of the x = 1−4 complexes, all water molecules bond with their dipole moment pointing away from the central metal cation, i.e., with the electronegative oxygen pointing toward the metal. These structures are in agreement with those found previously in the literature.[10,11] The $Ba^{2+}(H_2O)_2$ structure has an O−Ba−O angle of 122.4° with C_2 symmetry. This is similar to the dihydrated complexes of Ca^{2+} and Sr^{2+}, whereas that for Mg^{2+} is linear.[10,11,17,19] These bent geometries occur because the core electrons on the metals polarize away from the water ligands, essentially occupying a coordination site. The least polarizable alkaline earth dication, Mg^{2+}, cannot do this easily. The steric hindrance between the water ligands and the polarized core electrons then determines the GS geometry. This is also evident for the (3,0) system

DOI: 10.1021/acs.jpca.5b01087
J. Phys. Chem. A 2015, 119, 3800−3815

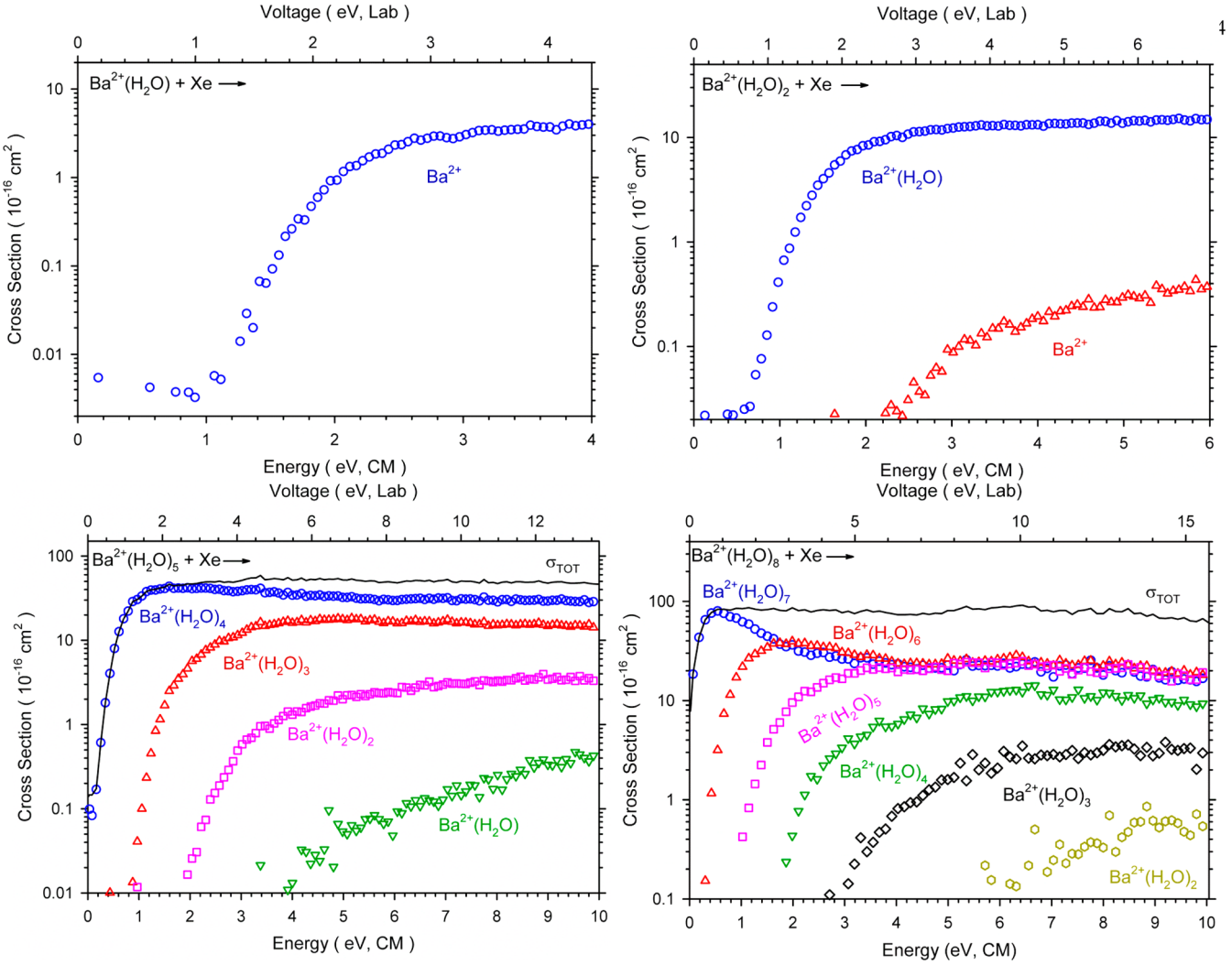

Figure 1. Cross sections for collision-induced dissociation of $Ba^{2+}(H_2O)_x$ where x = 1, 2, 5, and 8 (parts a, b, c, and d, respectively) with xenon at ≈0.2 mTorr as a function of kinetic energy in the CM frame (lower x-axis) and the laboratory frame voltage (upper x-axis).

where the lower polarizability of Mg^{2+} and Ca^{2+} lead to planar, D_3 symmetry geometries, whereas C_3 symmetric pyramidal structures are predicted for both Sr^{2+} and Ba^{2+}.[11,17,19,20] Upon the addition of a fourth water molecule, $M^{2+}(H_2O)_4$, all alkaline earth metals examined favor a tetrahedral structure with respect to the oxygen atoms with near S_4 symmetry.[11,17,19,20] Note that the water ligands in these structures are tilted to enable weak hydrogen bonding interactions between adjacent ligands.

Ba−O bond distances increase as the number of water ligands increases: 2.602, 2.647, 2.680, and 2.712 Å for x = 1, 2, 3, and 4, respectively, Table S3 of the Supporting Information. This is consistent with the decrease in $Ba^{2+}-OH_2$ bond strength as the hydration number increases.

Geometries involving second shell ligands were briefly examined for x = 1−4; however, such structures were not found to be energetically competitive, consistent with results for the lighter alkaline earth metal dications where such structures were unimportant until five water molecules are present.[17,19,20] For example, the $Ba^{2+}(H_2O)_2$ complex has a structure with a linear chain of water ligands that was found to be 38−47 kJ/mol (Level/SDD/def2-TZVPP//B3LYP/SDD/def2-TZVP where Level indicates B3LYP, B3P86, M06, and MP2(full)) higher in energy than the complex with both waters

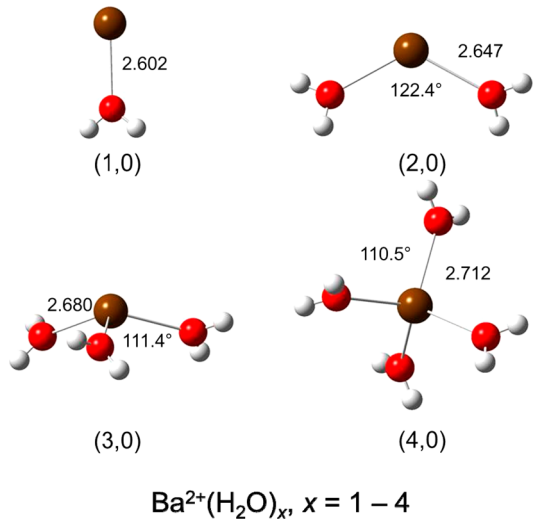

Figure 2. Ground geometries for the $Ba^{2+}(H_2O)_x$, x = 1−4 complexes, calculated at the B3LYP/SDD/def2-TZVP level of theory. Angles are between water molecules for (2,0), (3,0), and (4,0). Bond lengths (Ba−O) are listed in angstroms.

DOI: 10.1021/acs.jpca.5b01087
J. Phys. Chem. A 2015, 119, 3800−3815

Table 1. Relative Free Energies (Kilojoules per Mole) at 0 (298) K for $Ba^{2+}(H_2O)_x$ (x = 5−8) Isomers[a]

x	complex	B3LYP	B3P86	M06	MP2(full)
5	(5,0)	**0.0 (0.0)**	**0.0 (0.0)**	**0.0 (0.0)**	**0.0 (0.0)**
	(4,1)_2D_AA	12.0 (17.6)	8.9 (14.4)	11.9 (17.5)	14.6 (20.1)
	(4,1)_D_A	17.3 (18.2)	14.1 (14.9)	23.0 (23.9)	23.0 (23.8)
6	(6,0)	**0.0 (0.0)**	**0.0 (0.0)**	**0.0 (0.0)**	**0.0 (0.0)**
	(5,1)_2D_AA	6.3 (17.4)	3.0 (14.1)	6.2 (17.3)	9.8 (20.9)
	(5,1)_D_A	14.2 (16.6)	10.8 (13.2)	16.4 (18.8)	19.8 (22.2)
7	(7,0)	6.6 (3.1)	8.8 (5.2)	2.2 (**0.0**)	1.8 (**0.0**)
	(7,0)_C_2	4.6 (4.2)	7.0 (6.5)	**0.0** (0.9)	**0.0** (1.3)
	(6,1)_2D_AA	**0.0** (0.8)	**0.0** (0.7)	8.2 (10.3)	3.2 (5.7)
	(6,1)_D_A	7.6 (**0.0**)	7.7 (**0.0**)	19.8 (13.5)	12.9 (7.0)
8	(8,0)	15.8 (8.3)	20.8 (13.2)	**0.0 (0.0)**	0.8 (**0.0**)
	(7,1)_2D_AA	7.1 (1.6)	9.6 (4.1)	0.4 (2.5)	**0.0** (1.3)
	(6,2)_4D_2AAadjacent	**0.0 (0.0)**	**0.0 (0.0)**	4.9 (12.4)	**0.0** (6.8)
	(6,2)_4D_2AAacross	2.7 (3.8)	2.5 (3.6)	4.4 (13.1)	2.3 (10.3)
	(6,2)_DD,2D_2AA	3.7 (1.4)	4.0 (1.6)	8.6 (13.8)	4.0 (8.5)
	(6,2)_3D_AA,A[b]	9.8 (3.2)	10.1 (3.5)	19.5 (20.4)	12.4 (12.5)
	(6,1.5,0.5)_3D_AAD_AA	12.4 (11.1)	12.6 (11.3)	17.3 (23.5)	11.8 (17.3)

[a]Relative ΔG_{298} values are in parentheses. Bold values represent the predicted ground structures (GS). Single-point energies are calculated at the level shown with a SDD/def2-TZVPP basis set using B3LYP/SDD/def2-TZVP geometries and ZPE corrections. [b]An imaginary vibrational frequency leading to the (6,2)_4D_2AAadjacent structure was present for this structure.

attached directly to the metal. Some of these complexes are of interest in the context of the charge separation reaction and are discussed more fully below.

3.3. Theoretical Geometries for $Ba^{2+}(H_2O)_x$ Complexes, x = 5−8. For the larger complexes, x = 5−8, a number of alternative geometries and their single-point energies were explicitly examined to ensure that the GS was found. In the nomenclature used here, (a,b) denotes the number of water molecules present in the first (a) and second (b) solvent shells. If a water molecule binds in multiple shells, the value of 0.5 is included for both shells involved. To specify the hydrogen bonds formed between the different shells, inner shell water molecules can act as single (D) or double (DD) donors to waters in the outer shells, where the ligands can either be single (A) or double (AA) acceptors. For the x = 5−8 complexes, Table 1 lists the computed relative energies of several low-lying isomers. (Values including empirical dispersion corrections are listed in Table S2 of the Supporting Information.) A list of bond lengths for all GSs calculated at the B3LYP/SDD/def2-TZVP, B3LYP/SDD/def2-TZVPP, B3LYP-GD3BJ/SDD/def2-TZVPP, and B3LYP/DHF/def2-TZVPP levels of theory can be found in the Supporting Information, Table S3. These bond lengths are very similar for the different levels of theory except that the dispersion corrections shorten the bonds by 0−0.025 Å for first shell and 0.033−0.045 Å for second shell water molecules.

The GS for the $Ba^{2+}(H_2O)_5$ water complex is (5,0) with C_{2v} symmetry at all levels of theory, consistent with the analogous complexes of other alkaline earth metals.[17−20] Water ligands have a square pyramidal orientation with respect to the oxygen atoms, Figure 3. Two other geometries were examined, both (4,1), which have an inner shell of four water molecules with two different binding motifs for the secondary shell. The second shell water ligand can form either a single hydrogen bond with the inner shell (D_A) or two hydrogen bonds to separate inner shell water molecules (2D_AA). The (4,1)_2D_AA structure lies 9−15 kJ/mol above the (5,0) GS at 0 K and 14−20 kJ/mol at 298 K because the outer shell double acceptor water is restricted in its rotation. When the outer shell water molecule is less restricted, the (4,1)_D_A structure lies 14−23 kJ/mol above the (5,0) structure at 0 K and 15−24 kJ/mol at 298 K. Previous literature studies of this complex were limited to the (5,0) structure.[11]

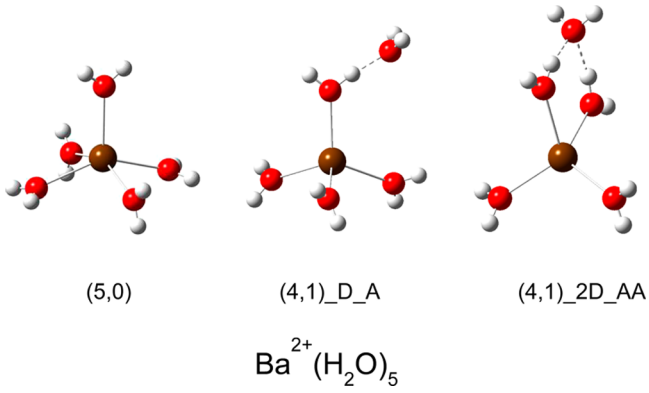

Figure 3. Low-lying isomers and ground geometries for $Ba^{2+}(H_2O)_5$ calculated at the B3LYP/SDD/def2-TZVP level of theory.

$Ba^{2+}(H_2O)_6$ has a (6,0) GS at all levels of theory. The structure is octahedral with respect to the oxygen atoms but has near T_h symmetry including the hydrogen atoms, Figure 4. The T_h symmetry results from weak hydrogen bonding interactions between adjacent water molecules. Additional isomers, (5,1)_2D_AA and (5,1)_D_A, were 3−10 and 11−20 kJ/mol higher in energy than the GS at 0 K, respectively, and 14−21 and 13−22 kJ/mol higher at 298 K. These results are similar to hexahydrate complexes for the other alkaline earth metals, except for Mg^{2+}, where B3LYP calculations place the (5,1)_2D_AA structure lower than (6,0) at 298 K, although MP2(full) still favors the (6,0) structure.[17]

For the $Ba^{2+}(H_2O)_7$ complex, Figure 5, the GS is dependent on the level of theory. B3LYP and B3P86 levels of theory favor the (6,1) structures with the (6,1)_2D_AA structure favored at 0 K and the (6,1)_D_A structure (which has a nearly free rotor for the outer shell water) favored slightly at 298 K. Both M06 and MP2(full) favor (7,0) structures with a structure having C_2

DOI: 10.1021/acs.jpca.5b01087
J. Phys. Chem. A 2015, 119, 3800−3815

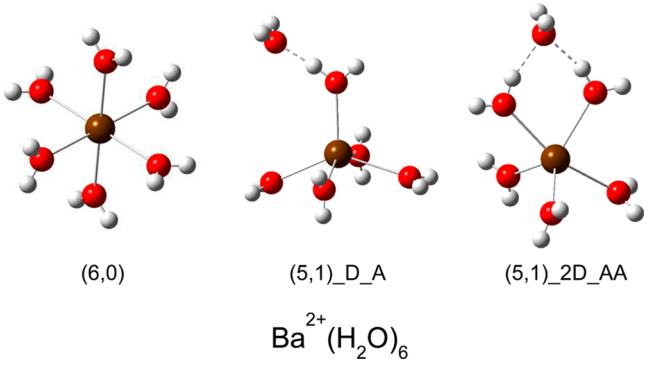

Figure 4. Low-lying isomers and ground geometries for $Ba^{2+}(H_2O)_6$ calculated at the B3LYP/SDD/def2-TZVP level of theory.

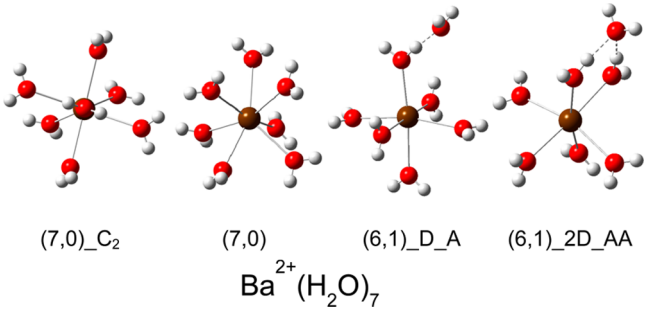

Figure 5. Low-lying isomers and ground geometries for $Ba^{2+}(H_2O)_7$ calculated at the B3LYP/SDD/def2-TZVP level of theory.

symmetry, (7,0)_C_2, favored by 2 kJ/mol over an unsymmetrical (7,0) structure, which becomes the GS at 298 K but only by 1 kJ/mol. (A close examination of these two structures indicates that they are distinct species and fully converged although no TS for their interconversion was located.) For B3LYP and B3P86, the (7,0) structures lie 3−9 kJ/mol above the (6,1) GS at both 0 and 298 K, whereas the (6,1) structures lie 3−20 kJ/mol above the (7,0) structures for the M06 and MP2(full) levels.

Assigning the GS for the $Ba^{2+}(H_2O)_8$ complex is more involved than the smaller complexes; seven distinct structures were examined, with six of these shown in Figure 6. Similar to the seven-water complex, a GS of $Ba^{2+}(H_2O)_6(H_2O)_2$ with six

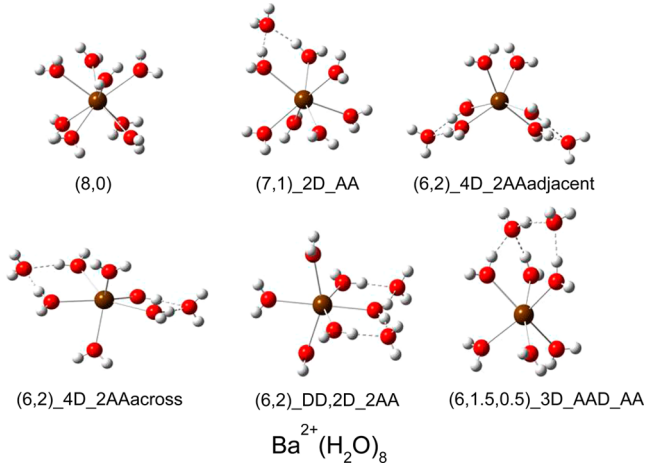

Figure 6. Low-lying isomers and ground geometries for $Ba^{2+}(H_2O)_8$ calculated at the B3LYP/SDD/def2-TZVP level of theory.

water ligands bound directly to Ba^{2+} is favored for B3LYP and B3P86 at both 0 and 298 K. This (6,2)_4D_2AAadjacent structure has two second shell ligands, both of which act as double acceptors with separate pairs of first shell waters located next to one another (as opposed to being across from one another in (6,2)_4D_2AAacross or sharing an inner shell donor as in (6,2)_DD,2D_2AA). At the MP2(full) level of theory, this (6,2) structure is only 0.02 kJ/mol higher in energy than the predicted (7,1) GS at 0 K, which changes to the (8,0) complex when 298 K thermal corrections are taken into account. The M06 level of theory once again predicts direct bonds to the central metal atom to be more favorable than the hydrogen bonds formed by a secondary ligand shell, leading to a predicted (8,0) GS at both 0 and 298 K. Additional structures located include (6,1.5,0.5)_3D_AAD_AA, in which one water bridges between first and second shell ligands, Figure 6, and (6,2)_3D_AA,A, which has a single acceptor ligand in the second shell that exhibits an imaginary frequency that takes it to (6,2)_4D_2AAadjacent.

The number of low-lying isomers close in relative free energy at 298 K suggests that multiple forms of the complex might be present in our thermalized ion beam. We can calculate an equilibrated Maxwell−Boltzmann distribution of our predicted structures for x = 7 and 8 (where all (6,1), (7,0), and (6,2) structures are combined for simplicity) at 298 K. For the x = 7 water complex, B3LYP and B3P86 predict populations of 79 and 90% for the (6,1) structures, whereas (7,0) structures represent 21 and 10%, respectively. The M06 and MP2(full) level of theory results indicate a majority of the (7,0) structures at 99 and 91% compared to 1 and 9%, respectively, for the (6,1) structures. For the x = 8 complex, B3LYP and B3P86 populations are dominated by the (6,2) structures, 79 and 91%, respectively, along with 20 and 9% of (7,1), and 1 and 0% for (8,0). The M06 and MP2(full) calculations show the opposite composition, leading to populations of 1 and 7% for (6,2), 26 and 35% for (7,1), and 72 and 58% for the (8,0) structure, respectively.

Overall, it can be seen that the B3LYP and B3P86 levels of theory favor smaller first shells than MP2(full), which in turn predicts smaller shells than the M06 level of theory. Previous infrared photodissociation studies of $Zn^{2+}(H_2O)_x$ complexes in this same size range demonstrated that the B3LYP and B3P86 predictions were inaccurate, whereas MP2 results accurately predicted the structures observed experimentally.[64] M06 structures paralleled the MP2 results but were not in good quantitative agreement with the binding energies determined in another related study.[21]

When compared to results for other alkaline earth metals, it is clear that the predicted size of the first shell is dependent on the size of the alkaline earth metal. As the metal gets larger, the water ligands are further apart, leading to less H_2O−H_2O repulsion and weaker hydrogen bonding, leading to potentially larger inner shell sizes. Thus, there is evidence that Mg^{2+} has an inner shell of six water ligands with five water ligands possible at 298 K and evidence for the presence of a four water inner shell contributing at higher temperatures (>353 K),[7,8,17] whereas Ca^{2+} and Sr^{2+} clearly prefer an inner shell of six, and the inner shell of Ba^{2+} may increase to seven or eight water molecules depending on the level of theory.[17−20]

3.4. Thermochemical Results for Primary Water Loss from $Ba^{2+}(H_2O)_x$ Complexes, x = 1−8. The total cross sections for the hydrated complexes with x = 1−8 were modeled using the empirical threshold model of eq 1 with the

DOI: 10.1021/acs.jpca.5b01087
J. Phys. Chem. A 2015, 119, 3800−3815

Table 2. Parameters of Eq 1 Used to Model Total Cross Sections for Collision-Induced Dissociation of $Ba^{2+}(H_2O)_x$, $x = 1-8$ and Entropies of Dissociation[a]

reactant[b]	product	σ_0[c]	n[c]	E_0 (PSL) (eV)[c]	E_0 (eV)[d]	$\Delta S^{\dagger}_{1000}$ (J/mol K)
(1,0)	(0,0)	7 (1)	1.3 (0.2)	1.75 (0.05)	1.75 (0.04)	22 (2)
(2,0)	(1,0)	22 (3)	0.9 (0.1)	1.50 (0.07)	1.51 (0.08)	−2 (5)
(3,0)	(2,0)	39 (4)	0.8 (0.1)	1.33 (0.04)	1.38 (0.05)	21 (5)
(4,0)	(3,0)	54 (6)	0.8 (0.1)	1.11 (0.04)	1.25 (0.05)	0 (5)
(5,0)	(4,0)	62 (9)	0.9 (0.1)	0.95 (0.07)	1.08 (0.07)	40 (5)
(6,0)	(5,0)	88 (16)	0.9 (0.1)	0.80 (0.06)	1.01 (0.05)	30 (5)
(6,1)_D_A	(6,0)	99 (7)	1.0 (0.1)	0.54 (0.05)	0.91 (0.06)	17 (4)
(7,0)	(6,0)	99 (11)	1.1 (0.1)	0.57 (0.06)	0.91 (0.06)	37 (16)
(6,2)adjacent	(6,1)_2D_AA	97 (4)	0.9 (0.1)	0.54 (0.03)	0.90 (0.04)	86 (5)
(7,1)	(7,0)_C_2	97 (4)	0.9 (0.1)	0.48 (0.04)	0.90 (0.04)	77 (4)
(8,0)	(7,0)_C_2	97 (9)	0.9 (0.1)	0.46 (0.07)	0.90 (0.04)	47 (10)

[a]Uncertainties (in parentheses) are reported to two standard deviations (95% confidence interval). [b]$Ba^{2+}(H_2O)_a(H_2O)_b$ reactant has (a,b) structure, see text. [c]Parameters from eq 1 with lifetime effects taken into account. [d]Threshold values from eq 1 when lifetime effects are not taken into account ($P_{D1} = 1$).

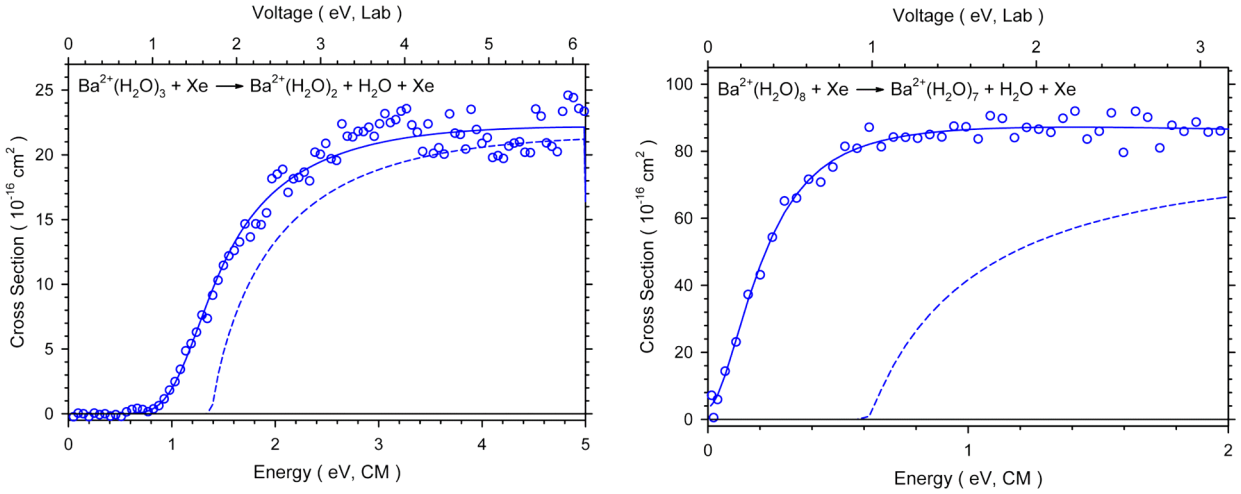

Figure 7. Zero-pressure extrapolated total cross sections for CID of $Ba^{2+}(H_2O)_x$ where $x = 3$ and 8 with xenon. Graphs shown as a function of kinetic energy in the CM frame (lower x-axis) and the laboratory frame voltage (upper x-axis). Solid lines represent the best fit to the data using eq 1 convoluted over the neutral and ion kinetic and internal energy distributions. Dashed lines show the models in the absence of experimental kinetic energy broadening for reactants having an internal energy of 0 K.

optimal modeling parameters listed in Table 2. The total cross section is modeled to avoid complications associated with the sequential dissociation channels that occur at higher kinetic energies. Data has been modeled with (eq 1) and without (eq 1 with $P_{D1} = 1$) lifetime effects to quantify the kinetic shifts, which increase as the $Ba^{2+}(H_2O)_x$ complexes increase in size, 0.00 eV for $x = 1$ to 0.44 eV for $x = 8$, where the latter value also depends on which structures are assumed for the reactant and product. The models of eq 1 are shown compared to the zero-pressure extrapolated cross sections in Figure 7 for complexes $x = 3$ and 8. Similar results for all complexes can be found in the Supporting Information, Figure S2. It can be seen that the models reproduce the data well from the threshold to 2−5 eV and over 1−2 orders of magnitude in cross section. All modeling is done utilizing molecular parameters for the B3LYP/SDD/def2-TZVP structures discussed above. Vibrational frequencies calculated at this level are <0.5% different compared to those obtained for selected structures at the B3LYP/DHF/def2-TZVPP level of theory.

For the $x = 1-6$ complexes, the theoretical results suggest there will be no appreciable population of excited isomers at 298 K. For the $x = 7$ and 8 complexes, different levels of theory find different ground structures and, in some cases, indicate that there may be multiple low-energy isomers populated. For these two systems, the data were analyzed assuming all possible ground structures located, Table 2. (Combinations of reactants and products for $x = 8$ other than those given in Table 2 were also tried but gave threshold values in this same range.) These alternative ground structures lead to slightly different threshold energies (although within the reported experimental uncertainties) because the kinetic shifts differ for the different structures.

3.5. Thermochemical Results for Sequential Modeling of $Ba^{2+}(H_2O)_x$ Complexes, $x = 1-8$. Modeling of both the primary and secondary water loss channels is accomplished using the sequential model, discussed above. This model includes simultaneous reproduction of the cross sections for the products formed in reactions 4 and 6.

$$Ba^{2+}(H_2O)_x + Xe \rightarrow Ba^{2+}(H_2O)_{x-2} + 2H_2O + Xe \quad (6)$$

Figure 8 and Figure S3 of the Supporting Information show that the sequential modeling analysis accurately reproduces both product cross sections in the threshold regions over extended energy and magnitude ranges. The modeling

DOI: 10.1021/acs.jpca.5b01087
J. Phys. Chem. A 2015, 119, 3800−3815

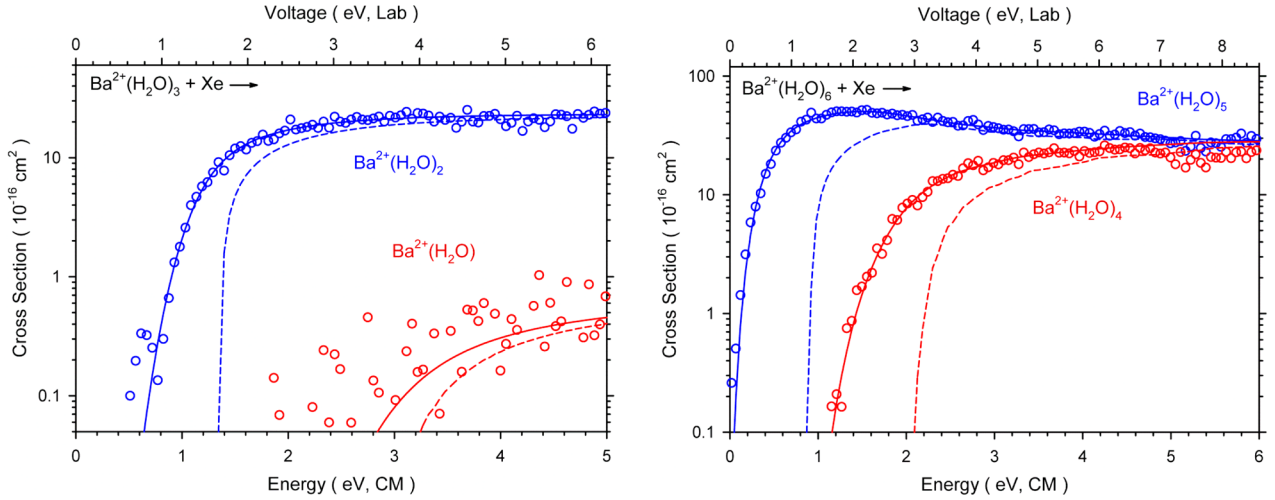

Figure 8. Zero-pressure extrapolated total cross sections for CID of $Ba^{2+}(H_2O)_x$ where x = 3 and 6 with xenon. Graphs shown as a function of kinetic energy in the CM frame (lower x-axis) and the laboratory frame voltage (upper x-axis). Solid lines show the best fit to data with the sequential model convoluted over the neutral and ion kinetic and internal energy distributions. Dashed lines represent the model cross sections in the absence of kinetic energy broadening for reactants having an internal energy of 0 K.

Table 3. Parameters of Eq 1 for Sequential Modeling of Collision–Induced Dissociation of $Ba^{2+}(H_2O)_x$, x = 2–8[a]

reactant[b]	product	σ_0	n	E_0 (PSL) (eV)[c]	E_0 (PSL) (eV)[d]
(2,0)	(1,0)	22 (2)	0.8 (0.1)	1.51 (0.05)	1.50 (0.07)
	(0,0)	1 (<1)		3.47 (0.37)	3.25 (0.09)
(3,0)	(2,0)	40 (4)	0.8 (0.1)	1.33 (0.03)	1.33 (0.04)
	(1,0)	2 (1)		3.01 (0.31)	2.83 (0.04)
(4,0)	(3,0)	53 (4)	0.9 (0.1)	1.08 (0.04)	1.11 (0.04)
	(2,0)	5 (2)		2.66 (0.07)	2.44 (0.06)
(5,0)	(4,0)	60 (7)	1.0 (0.1)	0.93 (0.04)	0.95 (0.07)
	(3,0)	28 (4)		2.29 (0.06)	2.06 (0.08)
(6,0)	(5,0)	85 (16)	1.0 (0.1)	0.78 (0.05)	0.80 (0.06)
	(4,0)	60 (12)		1.86 (0.06)	1.75 (0.09)
(6,1)_D_A	(6,0)	98 (15)	1.1 (0.1)	0.53 (0.05)	0.54 (0.05)
	(5,0)	93 (17)		1.38 (0.05)	1.34 (0.08)
(6,2)adjacent	(6,1)_2D_AA	97 (6)	0.9 (0.1)	0.52 (0.03)	0.54 (0.05)
	(6,0)	84 (6)		1.21 (0.07)	1.08 (0.07)

[a]Uncertainties (in parentheses) are reported to two standard deviations. [b]$Ba^{2+}(H_2O)_a(H_2O)_b$ reactant has (a,b) structure, see text. [c]Thresholds for sequentially modeled first and second water loss channels. [d]Experimental values from Table 2.

parameters that best represent the cross sections for sequential water loss are listed in Table 3. Because the total cross section determines the values of the parameter n needed to reproduce the data, the sequential model yields thresholds for loss of the first water that are essentially identical to those obtained from fitting the total cross section. The largest difference found for E_0 values between single channel and sequential modeling is 0.03 eV for the $Ba^{2+}(H_2O)_4$ complex, well within our experimental uncertainty.

The constraint on n also allows the secondary cross sections to be modeled even when the data are scattered because of low intensities, such as for x = 2 and 3. Thresholds for loss of a second water molecule determined from the sequential modeling are compared with values determined from the primary thresholds in Table 3. It can be seen that the sequential modeling always yields values higher than the sum of primary threshold energies, a result also typical for other hydrated alkaline earth systems.[17,19] This is probably a consequence of somewhat inaccurately assessing how energy is distributed after the initial dissociation. Nevertheless, for the largest complexes, x = 6–8, the differences in these secondary threshold values are 0.05–0.15 eV, within the combined experimental uncertainties. For the smaller complexes, x = 2–5, differences increase to 0.18–0.25 eV. This is again within experimental uncertainty for the smallest complexes, x = 2 and 3, but only because the relatively noisy data for the secondary water loss channel leads to large uncertainties in the secondary thresholds. Notably, the difference between the threshold energies for primary and secondary water loss yields a completely independent set of BDEs, which we will refer to as secondary BDEs, as discussed further below.

Another indication that the sequential model may not accurately determine the distributions of energies in the initial dissociation is the need to independently scale the secondary cross sections (different $\sigma_{0,j}$ values for the primary and secondary channels). If the assumed statistical model accounted for these energy distributions precisely, then the $\sigma_{0,j}$ values for both channels would be equal, Table 3. The need for independent scaling factors is consistent with previous results[50] suggesting that the sequential model is inexact. However, we note that the scaling factors for the smaller complexes differ the

DOI: 10.1021/acs.jpca.5b01087
J. Phys. Chem. A 2015, 119, 3800–3815

Table 4. Relative 0 K Energies (Kilojoules per Mole) for Charge Separation Transition States, Intermediates, and Products for CID of $Ba^{2+}(H_2O)_2$[a]

complex	B3LYP	B3P86	M06	MP2(full)	B3LYP[b]	MP2
$Ba^{2+}(H_2O) + H_2O$	146	147	147	144	141	141[c]
$Ba^{2+}(H_2O)_2$ (2,0)	0	0	0	0	0	0[c]
TS1	44	42	46	43	41	
INT(1,1)	41	38	47	42	40	44 (40)[d]
TS[0 + 1]	158	153	160	174	162	174 (175)[d]
$BaOH^+ + H_3O^+$	−27	−38	−27	−7	−19	−26[c]

[a]Geometries and vibrational frequencies calculated at the B3LYP/SDD/def2-TZVP level with single-point energies calculated at the level shown with the def2-TZVPP basis set including ZPE corrections. [b]B3LYP/SDD/6-311+G(3df,2pd) values from ref 13. [c]MP2/ATZ ZPE corrected values from ref 16. [d]MP2/ADZ values from ref 16 corrected with current scaled ZPEs. Uncorrected values are in parentheses.

most but are fairly similar for the larger complexes, i.e., the latter behave more ergodically.

3.6. Conversion of 0 K Hydration Energies to 298 K. Converting 0 K hydration energies to enthalpies and free energies at 298 K is done by calculating $H_{298} - H_0$ and $T\Delta S_{298}$ values using the rigid rotor−harmonic oscillator approximation with the rotational constants and vibrational frequencies calculated at the B3LYP/SDD/def2-TZVP level of theory. These values can be found in Table S4 of the Supporting Information. Uncertainties are found by scaling the vibrational frequencies up and down by 10%. It is worth noting that the low-frequency torsional motions of the water ligands may not be described accurately by the harmonic approximation.

3.7. Charge Separation of $Ba^{2+}(H_2O)_2$. As noted in the Introduction, the hydrated complexes of Ca^{2+} and Sr^{2+} undergo the charge separation reaction exclusively for the $M^{2+}(H_2O)_2$ complex, whereas this process is observed for both $x = 3$ and 4 for Mg^{2+}.[17,19,20] Despite careful examination, charge separation to form barium hydroxide cation and protonated water is not observed experimentally from the $Ba^{2+}(H_2O)_2$ complex. To understand this failure, the dissociation pathways of the $Ba^{2+}(H_2O)_2$ complex by loss of water and charge separation were examined. Geometry optimizations for each pathway were performed at the B3LYP/SDD/def2-TZVP level of theory, locating structures similar to those previously determined for the analogous Ca^{2+} and Sr^{2+} systems.[19,20] Using these geometries, single-point energies at the B3LYP, B3P86, M06, and MP2(full) levels of theory with a def2-TZVPP basis set were computed, as listed in Table 4 along with similar results from Beyer et al.[13] and Miliordos and Xantheas.[16] Figure S4 of the Supporting Information shows B3LYP results from the current study.

For $Ba^{2+}(H_2O)_2$, charge separation is a two-step process in which an inner shell water transfers to the second shell and then a covalent O−H bond is cleaved. The (1,1) intermediate is 38−47 kJ/mol higher in energy than the (2,0) GS. These are separated by TS1, which is only 1−4 kJ/mol higher in energy than the INT (1,1), except at the M06 level of theory where the TS is lower by 1 kJ/mol. From INT(1,1), product formation occurs over a large Coulomb barrier, the rate-limiting step, of 153−174 kJ/mol before forming the $BaOH^+ + H_3O^+$ products. At all levels of theory, the energy required for simple water loss from $Ba^{2+}(H_2O)_2$ is lower than that for the charge separation TS by 6−33 kJ/mol, Table 4. All levels of theory also agree that the $Ba^{2+}(H_2O)_2$ species is metastable with the $BaOH^+ + H_3O^+$ species lying 7−38 kJ/mol lower in energy. Thus, the failure to observe charge separation from $Ba^{2+}(H_2O)_2$ is a consequence of this channel being both enthalpically and entropically disfavored compared to loss of the water ligand. This failure to observe the $BaOH^+$ and H_3O^+ fragments is also illustrated by our ability to generate the $Ba^{2+}(H_2O)$ complex in our source by fragmenting larger complexes. In contrast, formation of $M^{2+}(H_2O)$ complexes where M = Mg and Ca was not possible because the larger complexes of these metals preferentially decompose by charge separation processes instead of water loss.[17,19]

3.8. Charge Separation of $Ba^{2+}(H_2O)_3$. Interestingly, although charge separation products were not observed for the $Ba^{2+}(H_2O)_2$ + Xe reaction, a very small amount of $BaOH^+$, barely above the noise level, was observed in the reaction of $Ba^{2+}(H_2O)_3$ + Xe under specific source conditions and at a high pressure of Xe (0.19 mTorr), as shown in Figure 9. The low

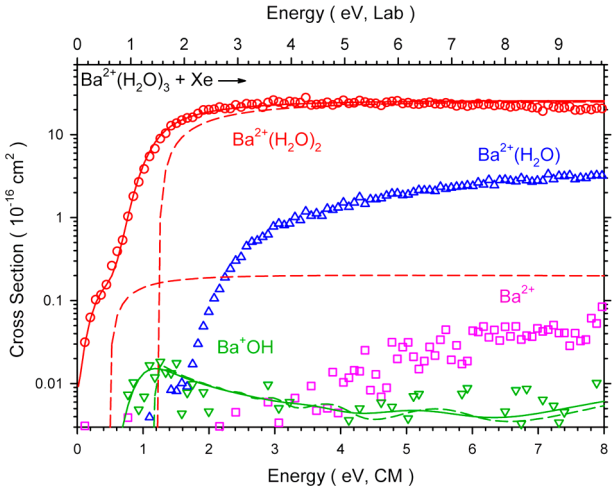

Figure 9. Cross sections for collision-induced dissociation of $Ba^{2+}(H_2O)_3$ with Xe at high pressure (0.19 mTorr), under source conditions that optimize intensity (open symbols). Dashed red lines are models of the cross section for water loss of the tail feature at low energy and from the thermalized reactants. The solid red line is the sum of both dashed red lines convoluted over the reactant kinetic and internal energy distributions and reproduces the cross section for loss of a single water. Green solid (convoluted) and dashed (unconvoluted) lines are the model of the $BaOH^+$ channel from a competitive analysis with the primary water loss channel from thermalized reactants, see text.

intensity (~three times the noise level and <0.1% of our largest product) hindered our ability to conduct a definitive experimental investigation and unfortunately meant that the accompanying solvated proton product, $H^+(H_2O)$ or $H^+(H_2O)_2$, could not be found. The latter failure is probably a result of the large kinetic energy release, as discussed above. The $BaOH^+$ product was observed only when the voltage

DOI: 10.1021/acs.jpca.5b01087
J. Phys. Chem. A 2015, 119, 3800−3815

applied to the dc electrodes that control the in-source fragmentation process was tuned to maximize the $Ba^{2+}(H_2O)_3$ intensity, which was *not* the electrode conditions needed to give the coldest distribution of complexes. Further examination of this phenomena can be found below.

A reaction coordinate pathway for $Ba^{2+}(H_2O)_3$ decomposing by both water loss and charge separation to $BaOH^+ + H_5O_2^+$ and $BaOH^+(H_2O) + H_3O^+$ can be found in Figure 10. Table 5 contains single-point energy values at each level of theory for the different structures located on the reaction coordinate pathway along with comparable results from Miliordos and Xantheas (MX).[16] Formation of $BaOH^+ + H_5O_2^+$ products requires a path involving three intermediates, (2,1), (1,2), and (1,1,1) structures, and four TSs connecting them to the final products. The final TS[0 + 2], where the numbers indicate the number of waters bound to the $BaOH^+$ and H^+ products, is the Coulomb barrier leading to formation of the $BaOH^+ + H_5O_2^+$ products. This charge separation channel is more favorable than simple water loss at the B3LYP and B3P86 levels of theory by 1 and 11 kJ/mol, respectively; whereas MP2 and M06 levels of theory predict the opposite, with the water loss pathway being favored by 17−23 kJ/mol, respectively. The MP2/ATZ results of MX parallel the present MP2 (full) values. Thus, this channel is entropically disfavored compared to water loss but is close to being energetically feasible.

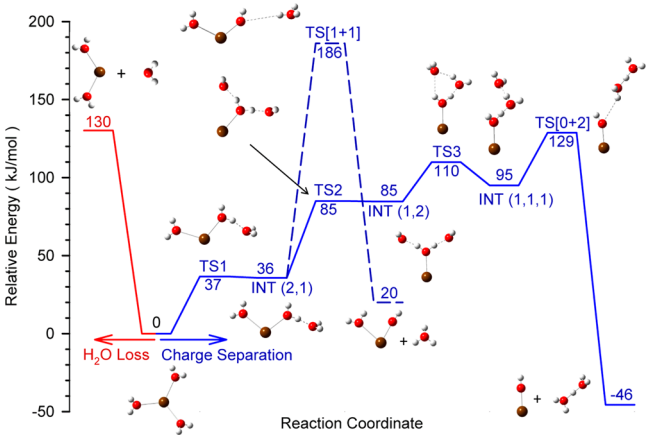

Figure 10. Reaction coordinates for water loss and two charge separation pathways of $Ba^{2+}(H_2O)_3$. Energies (kilojoules per mole) are calculated at the B3LYP/def2-TZVPP level of theory and include zero-point energies.

Table 5. Relative 0 K Energies (Kilojoules per Mole) for Charge Separation Transition States, Intermediates, and Products for CID of $Ba^{2+}(H_2O)_3$[a]

complex	B3LYP	B3P86	M06	MP2(full)	MP2
$Ba^{2+}(H_2O)_2 + H_2O$	130	130	130	131	135[b]
$Ba^{2+}(H_2O)_3$	0	0	0	0	
TS1	37	34	38	38	
INT(2,1)	36	33	38	38	38 (35)[c]
TS2	85	80	89	87	
INT(1,2)	85	79	89	88	
TS3	110	104	114	111	
INT(1,1,1)	95	87	104	98	
TS[0 + 2]	129	119	153	148	154 (159)[c]
$BaOH^+ + H^+(H_2O)_2$	−46	−58	−43	−22	−31[b]
TS[1 + 1]	186	181	202	187	211 (213)[c]
$BaOH^+(H_2O) + H_3O^+$	20	12	36	16	21[b]

[a]Geometries and vibrational frequencies are calculated at the B3LYP/SDD/def2-TZVP level, and single-point energies are calculated at the level shown with the SDD/def2-TZVPP basis set including ZPE corrections. [b]MP2/ATZ ZPE corrected values from ref 16. [c]MP2/ADZ values from ref 16 corrected with current works scaled ZPEs. Uncorrected values are in parentheses.

The pathway for $BaOH^+(H_2O) + H_3O^+$ formation goes through the (2,1) intermediate and has a single TS before product formation, TS[1 + 1]. This Coulomb barrier is higher than the barrier for water loss by 51−76 kJ/mol, 181−211 kJ/mol above $Ba^{2+}(H_2O)_3$. Note that the $BaOH^+(H_2O) + H_3O^+$ products are calculated to be 38−79 kJ/mol higher than the $BaOH^+ + H_5O_2^+$ products, such that even though the reverse Coulomb barriers are similar (166−190 versus 170−196 kJ/mol, respectively), the TS leading to the latter channel is favored by 39−62 kJ/mol.

Given these theoretical results, we modeled the cross sections shown in Figure 9, with details contained in Table S5 of the Supporting Information. The major feature in the cross section for loss of water to form $Ba^{2+}(H_2O)_2$ can be reproduced using a model similar to that for zero-pressure extrapolated data; however, the threshold needs to be lower by 0.1−0.2 eV to account for the effects of the higher pressure of Xe. The tail in this cross section can then be reproduced with a threshold (E_0 = 0.43 eV) that is 0.7 ± 0.1 eV lower in energy than the major cross section feature (E_0 = 1.16 eV) and a magnitude approximately 100 times smaller (i.e., ∼1% population). When competition between either of these water loss channels and charge separation over TS[0 + 2] is now included in the modeling, we find that the charge separation channel cross section can be reproduced from the $Ba^{2+}(H_2O)_3$ (3,0) GS, Figure 9. Note that the only adjustable parameter for this channel is the threshold because the shape of the cross section (parameter n) is controlled by the water loss channel and its magnitude is controlled by the statistical factors k_j/k_{tot} in eq 1. The excited (2,1), (1,2), and (1,1,1) isomers also yield this product, but with much lower intensities such that these contributions are negligible. The modeled data show that the threshold for charge separation is ∼0.1 eV lower than that for water loss. If the charge separation channel threshold energy is set above or equal to that for water loss, the magnitude of this entropically disfavored channel is much too small compared to experiment.

4. DISCUSSION

4.1. Comparison between TCID Primary and Secondary Experimental Values. The statistical model used to analyze energy-dependent cross sections for primary water loss has shown its accuracy over multiple studies.[17,19,24,25] Because detailed accounting of the energy distributions when two water molecules are lost is more complicated than that for a primary loss,[44] primary BDEs are considered more reliable. For the x = 7 and 8 complexes where multiple isomers are predicted to be the GS depending on the theoretical approach, the value obtained using the (7,0) complex is our preferred primary value because of infrared action spectroscopy results discussed below.[8] For x = 8, a median value of all thresholds with an increased uncertainty is utilized as our best primary value.

Comparing the secondary BDEs to the primary BDEs, Table 6 and Figure 11, we see that the former are systematically higher than the latter for all complex sizes. The mean absolute deviation (MAD) between primary and secondary values in this

DOI: 10.1021/acs.jpca.5b01087
J. Phys. Chem. A 2015, 119, 3800−3815

Table 6. Comparison of 0 K Enthalpy Values (Kilojoules per Mole) from Experiment, Theory, and the Literature for $Ba^{2+}(H_2O)_x$, x = 1−8

x	ΔH_0[a] (primary)	ΔH_0[a] (secondary)	HPMS[b]	BIRD[c]	B3LYP/DHF[d]	MP2(full)/DHF[d,e]	GF[f]	MP2[g]
1	169 ± 5	189 ± 36			167	162	166	165
2	145 ± 7	162 ± 27			145	143	148	141
3	129 ± 4	152 ± 7			128	128	134	135
4	107 ± 4	131 ± 4		107 ± 4	114	115	121	119
5	92 ± 6	105 ± 6	99 ± 4	88 ± 3	92	97	102	98
6	77 ± 5	82 ± 3	82 ± 4	75 ± 3	83	87	93	91
7	55 ± 6	66 ± 3	66 ± 4	64 ± 3	70	74		
8	48 ± 9		61 ± 4		70	69		
MADs[h]								
Primary		16 ± 7	9 ± 3	4 ± 3	7 ± 7	9 ± 7	9 ± 5	8 ± 4
Secondary			2 ± 3	10 ± 8	14 ± 8	15 ± 8	15 ± 8	15 ± 6
HPMS				7 ± 4	7 ± 6	5 ± 2	7 ± 4	5 ± 4
BIRD					6 ± 2	10 ± 1	15 ± 2	13 ± 2
B3LYP						3 ± 2	6 ± 3	5 ± 2
MP2(full)							5 ± 1	4 ± 2

[a]Experimental values from Tables 1 and 2. [b]High-pressure mass spectrometry values from ref 6 adjusted to 0 K. [c]Blackbody infrared dissociation values from ref 7 adjusted to 0 K. [d]Theoretical values utilize the DHF/def2-TZVPP basis set and are zero-point energy and counterpoise corrected. [e]B3LYP/DHF/def2-TZVPP geometries and vibrational frequencies. [f]MP2/HW*/6-31+G(d) values from Glendening and Feller, ref 11. [g]MP2/ATZ values from ref 16. [h]Mean absolute deviations.

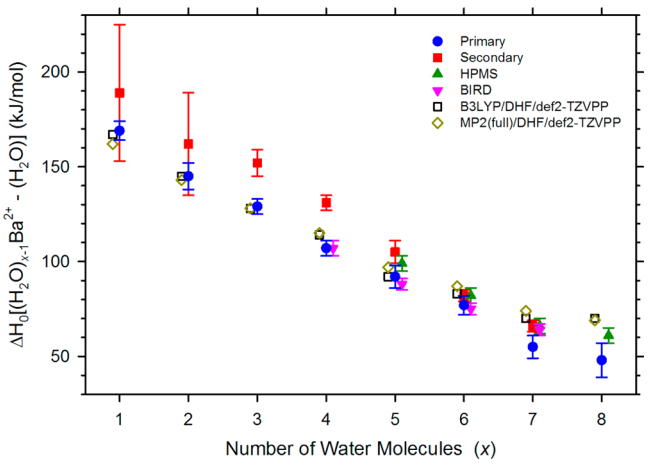

Figure 11. Comparison of experimental primary (solid blue circles) and secondary (solid red squares), computational (open symbols), and experimental literature (solid green and pink symbols) values for $Ba^{2+}(H_2O)_x$ bond energies at 0 K. All results are from Table 6. Data points for theory and literature values have been offset for clarity.

study is 16 ± 7 kJ/mol. Deviations for x = 5−7 range from 5−13 kJ/mol, but x = 1−4 have larger differences of 17−24 kJ/mol (with no systematic changes within these groups). For the smallest complexes, x = 1 and 2, the relatively noisy data for the secondary water loss channel leads to larger uncertainties in the secondary BDEs compared to those for the larger complexes. Previous studies also found the secondary BDEs to be systematically larger than the primary values, although the present differences are larger than the MADs reported for $Mg^{2+}(H_2O)_x$ (7 kJ/mol), $Ca^{2+}(H_2O)_x$ (12 kJ/mol), $Cd^{2+}(H_2O)_x$ (8 kJ/mol), and $Fe^{2+}(H_2O)_x$ (3 kJ/mol) complexes.[17,19,24,25] Fortunately in the current study, appreciable intensities of all complexes x = 1−8 were produced experimentally, allowing modeling of the primary water loss for all complexes.

4.2. Comparison between Present and Literature Experimental Values. Previous experimental work has determined $Ba^{2+}(H_2O)_x$ hydration enthalpies using HPMS, x = 5−14,[6] and BIRD, x = 4−7.[7] These values have been adjusted to 0 K values and are compared with the present values in Table 6 and Figure 11. TCID primary values show excellent agreement with BIRD[7] values with a MAD of 4 kJ/mol, and the largest difference being 9 kJ/mol for the x = 7 complex, within the combined experimental uncertainties. The HPMS[6] results range from 5−13 kJ/mol higher than our primary TCID values for the $Ba^{2+}(H_2O)_x$ complexes, x = 5−8, with a MAD of 9 kJ/mol. HPMS[6] results are systematically higher than both TCID and BIRD experimental values, such that these values more closely match our secondary values, with a MAD of only 2 kJ/mol.

In looking for experimental evidence of possible shell closings, we note that both TCID and HPMS results find that the bond energies level off between x = 7 and 8, and indeed that subsequent addition of water molecules up to x = 14 results in bond energies that differ by <4 kJ/mol for each step.[6] For hydrated complexes of the other alkaline earth metal dications,[17−19] similar results were interpreted as suggesting these ligands were in the second solvent shell and binding in similar positions (both AA) to inner shell ligands, i.e., the (6,1) and (6,2) structures, respectively. In the HPMS study, a 12 kJ/mol difference in 298 K bond enthalpies is measured for x = 6 and 7, three times that for subsequent additions of water up to x = 14. The present results also observe a slightly larger drop between x = 6 and 7 than for smaller complexes, which might also be consistent with closing the inner shell at six water ligands; however, our secondary values as well as the HPMS and BIRD results find smaller decreases, leading to ambiguity in experimentally assigning the inner shell size.

More compelling information comes from the infrared action spectra obtained by the Williams group at 170 K,[8] which are consistent with the presence of both the (6,1) and (7,0) structures. Very weak photodissociation at 3430 cm^{-1} is clearly evident in the experimental data and attributed to H_2O-H_2O interactions characteristic of second shell formation in (6,1); however, the weak intensity of this band and the relative intensities of the major free−OH stretching bands were

DOI: 10.1021/acs.jpca.5b01087
J. Phys. Chem. A 2015, 119, 3800−3815

interpreted to indicate that (7,0) is probably the dominant structure present.[8] This conclusion is consistent with the relative energies calculated at the M06 and MP2(full) levels, Table 1, where free energies at 170 K would suggest equilibrium populations for (7,0) of 98 and 69%, respectively. This conclusion disagrees with B3LYP and B3P86 results, where 170 K free energies predict equilibrium populations for the (7,0) structures of 17 and 8%, respectively. Notably for x = 8, the band at 3430 cm^{-1} increases appreciably, consistent with the presence of either (7,1) or (6,2) structures. This is consistent with all levels of theory, which predict populations for these isomers at 170 K of >47% (100% for B3LYP and B3P86).

Predicting the CN for $Ba^{2+}(H_2O)_x$ is more complicated than that for the other alkaline earth metals because of its large ionic radius (1.38 Å), 17% larger than that of Sr^{2+} (1.18 Å).[65] Peschke et al.[6] speculate that this decreases the steric hindrance between water molecules, thereby allowing the addition of a seventh water into the first solvent shell. In addition, this larger ionic radius leads to weaker $M^{2+}-OH_2$ bonds that approach those of the second shell AA interactions found in the (6,1) and (6,2) complexes. The similarities in these inner and outer shell BDEs limit our ability to definitively determine an inner shell CN size from the TCID data.

4.3. Comparison of Theoretical BDEs for $Ba^{2+}(H_2O)_x$, x = 1−8. As stated above, all levels of theory employed here agree on the GSs for the $Ba^{2+}(H_2O)_x$ complexes where x = 1−6. There is some disagreement on the GSs of the x = 7 and 8 complexes, Table 1. B3LYP and B3P86 agree with each other for all basis sets examined, whereas MP2(full) and M06 yield distinct results. In the following discussion, 0 K BDEs are determined from GS reactants going to predicted GS products at each different level of theory. For all complexes, x = 1−8, calculated BDEs are listed in Table S1 of the Supporting Information. Minor variations are found for the BDEs among the B3LYP, B3P86, M06, and MP2(full) levels of theory using the SDD/def2-TZVPP//SDD/def2-TZVP, SDD/def2-TZVPP, and DHF/def2-TZVPP basis sets. The differences range from 0−15 kJ/mol across the four levels of theory and three def2 basis sets with the largest differences found for the x = 1 and 7 water complexes. The latter discrepancies depend on variations in the GSs for x = 7. For each level of theory, calculated BDEs show a general trend of larger basis sets leading to greater BDEs.

Previous theoretical work was done by Glendening and Feller[11] at the MP2 level with a standard 6-31+G(d) basis set for O and H and a hybrid basis set for Ba that utilized HW*.[55] They found BDEs for x = 1−6 that essentially match the present MP2(full)/DHF/def2-TZVPP theoretical results without counterpoise corrections, with differences ranging from 1−4 kJ/mol and a MAD of only 2 ± 1 kJ/mol, Table S1 of the Supporting Information. Their values are 4−6 kJ/mol higher than the MP2(full)/DHF/def2-TZVPP theoretical values, with a MAD of 4 ± 2 kJ/mol, when counterpoise corrections are applied to the present results.

Kaupp and Schleyer[10] looked at x = 1 and 2 and determined BDEs with HF, MP2, and MP4 (x = 1 only) using a 6s6p2d basis set contraction followed by the 6s6p5d basis set for single-point energy calculations. Their MP2 values are larger than the present counterpoise uncorrected MP2(full)/DHF/def2-TZVPP values by 9−10 kJ/mol, Table S1 of the Supporting Information.[10]

Additional work performed by Miliordos and Xantheas examined hydration enthalpies for the x = 1−6 complexes and also did not include counterpoise corrections.[16] When their findings are compared with our uncorrected MP2(full)/DHF/def2-TZVPP results, differences range from 0−8 kJ/mol and associated MADs of 4 ± 3 and 3 ± 3 kJ/mol were found for their calculations done with the ADZ and ATZ basis sets, respectively, in Table S1 in the Supporting Information.

4.4. Comparison between Experimental and Theoretical Values. Our primary 0 K experimental enthalpy values are in reasonable agreement with those calculated at the different levels of theory with all the basis sets examined for x = 2−6, with differences ranging from 0−12 kJ/mol, Table S1 of the Supporting Information. In general, B3LYP and B3P86 calculations yield similar BDEs with B3P86 values being typically larger by 2−3 kJ/mol. MP2(full) results are slightly low for x = 1 but otherwise agree with B3LYP and B3P86 results. All three of these approaches predict that the x = 7 and 8 complexes have similar BDEs, as is observed experimentally. M06 results typically lie between those of B3LYP/B3P86 and MP2(full) from x = 1−6 but also predict that the BDEs for x = 6 and 7 are most similar, rather than x = 7 and 8. From these observations, we conclude that B3LYP, B3P86, and MP2(full) do the best job of duplicating our experimental BDEs across the x = 1−8 range. For simplicity, Figure 11 and Table 6 include the levels of theory that agree with experiment the best, B3LYP and MP2(full)/DHF/def2-TZVPP//B3LYP/DHF/def2-TZVPP. For x = 1, values from Level/SDD/def2-TZVPP//B3LYP/SDD/def2-TZVP are lower than experiment by 4−15 kJ/mol for all four levels of theory. Increasing the basis set size for both geometry optimization and single-point energy calculations to the DHF/def2-TZVPP basis set led to an improved reproduction of the $Ba^{2+}(H_2O)$ BDE, with differences decreasing to 0−7 kJ/mol. We believe that the discrepancy found for the smaller basis set may be associated with strong interactions between the core electrons on Ba^{2+} and the water ligand. Because the basis sets used here do not allow polarization of the core electrons, such a strong interaction can lead to underestimated bond energies, as previously documented for singly ligated Li^+ complexes.[66]

For the larger complexes of x = 7 and 8, the B3LYP/DHF/def2-TZVPP and MP2(full)/DHF/def2-TZVPP results have differences with experiment that are larger, 15−22 kJ/mol, with the experimental primary values (as well as HPMS and BIRD values) lying systematically lower than theory. Similar trends have been seen for the other alkaline earth metals[17,19] Overall, primary 0 K enthalpy values for water loss from x = 1−8 complexes agree well with the B3LYP and MP2(full) levels of theory, with MADs from experiment of 7 and 9 kJ/mol, respectively, Table 6. These differences are comparable to the mean uncertainty in the experimental values of 5 kJ/mol. The secondary 0 K enthalpy values have systematically larger MADs compared to theory of 14 and 15 kJ/mol, respectively. In most cases, not including the counterpoise corrections worsens the agreement between experiment and theory.

These comparisons utilize thresholds for x = 7 determined by modeling with the (7,0) structure and median results for the x = 8 complex. For the $Ba^{2+}(H_2O)_7$ complex, modeling with frequencies from the (6,1)_D_A and (7,0) structures yielded similar E_0 values, 52 and 55 kJ/mol, respectively, Table 2, such that the comparisons above change very little if the (6,1) structure reactant were used instead. Modeling $Ba^{2+}(H_2O)_8$ with frequencies from the three most likely structures, (6,2)

DOI: 10.1021/acs.jpca.5b01087
J. Phys. Chem. A 2015, 119, 3800−3815

_4D_2AAadjacent, (7,1)_2D_AA, and (8,0), yielded E_0 values of 52, 46, and 44 kJ/mol, respectively, Table 2, such that the median value of 48 kJ/mol is chosen. Theory predicts BDEs for $x = 8$ that exceed even the highest of these values, which could suggest but does not demonstrate that the (6,2) structure may dominate the ion population.

4.5. Evaluation of the Charge Separation Process. Charge separation is observed only when it is either enthalpically favored or nearly so compared to the energy needed to lose a water ligand. Because the energy for losing the water ligand gets larger as the size of the hydrated metal complex gets smaller, it can eventually surpass the Coulomb barrier height, thus allowing charge separation to be observed. (The barrier height for charge separation tends to be relatively static as it relies primarily on the Coulomb repulsion between the two positive ionic products, although some variations are observed depending on the stabilities of the products relative to the reactants. Thus, the Coulomb barriers for combining H_3O^+ with $CaOH^+$, $SrOH^+$, and $BaOH^+$ were calculated to be 195, 188, and 185 kJ/mol, respectively, at the B3LYP/6-311+G(2d,2p)//B3LYP/6-311+G(d,p) level for Ca and B3LYP/def2-TZVPP//B3LYP/def2-TZVPP level for Sr and Ba.) Therefore, the charge separation products appear with a critical size (x_c) of 3 (possibly 4) for Mg^{2+} down to $x_c = 2$ for Ca^{2+} and Sr^{2+}.[17,19,20] Being a larger dication, Ba^{2+} binds water more weakly than the smaller alkaline earth dications. Thus, on the basis of the previous results, charge separation is likely to occur only for the $Ba^{2+}(H_2O)_2$ complex, if at all.

As noted above, charge separation was not experimentally observed when examining the $Ba^{2+}(H_2O)_2$ water complex. This is entirely consistent with the current and literature[13,16] quantum chemical calculations, Table 4, which clearly show that the energy required for dissociation of a single water molecule is lower (by 6−33 kJ/mol) than that of the rate-limiting transition state (TS[0 + 1]) for the charge separation process, Table 4 and Figure S4 of the Supporting Information. Comparable calculations for the $Sr^{2+}(H_2O)_2$ system show that water loss is disfavored by 19 kJ/mol at the B3LYP/SDD/def2-TZVPP level and that the two channels are isoenergetic at the MP2(full)/SDD/def2-TZVPP level.[20] The latter result agrees better with the experimental observations, where the charge separation channel is observed but has a cross section that is over two orders of magnitude smaller than that for water loss.[20] Thus, the failure to observe formation of $BaOH^+ + H_3O^+$ from $Ba^{2+}(H_2O)_2$ is consistent with our previous experimental work on hydrated Sr^{2+} and the theoretical calculations.

When our source conditions were changed to allow for maximum signal intensity of the $Ba^{2+}(H_2O)_3$ reactant, it was possible to observe the $BaOH^+$ product, which theory shows is accompanied by $H_5O_2^+$. These data, shown in Figure 9, also exhibit evidence of reactants that are not fully thermalized in the form of a low-energy feature in the cross section of the primary product. Modeling of this feature suggests the excited species lie ∼70 kJ/mol above the GS, see Table S5 of the Supporting Information. This energy is somewhere between the calculated energies of the (2,1) and (1,2) isomers, 33−38 and 79−89 kJ/mol, respectively. The $H_5O_2^+$ product has not been observed in previous studies of the other alkaline earth metals,[17,19,20] although hydrated transition-metal dications do dissociate to form this species.[22,23,25] The observations that the charge separation pathway in Figure 10 is complex and that this pathway has a similar energy barrier as water loss are also consistent with our experimental observation that charge separation is an inefficient competitive pathway. B3LYP and B3P86/SDD/def2-TZVPP//B3LYP/SDD/def2-TZVP calculations indicate formation of $BaOH^+$ is favored by 1 and 11 kJ/mol, respectively. MP2(full) and M06 levels of theory show that water loss is favored by 17 and 23 kJ/mol, such that charge separation should not be observed, in contrast to experimental findings. Even though the two processes may be energetically competitive, the water loss pathway has a loose TS whereas charge separation is a multistep process involving tight TSs, making the latter kinetically disfavored and therefore much smaller in magnitude. This effect is shown quantitatively by the modeling in Figure 9.

5. CONCLUSION

Experimental cross sections for collision-induced dissociation of $Ba^{2+}(H_2O)_x$ complexes, where $x = 1−8$, with Xe have been examined using GIBMS. Larger complexes, $x = 6−8$, are generated directly from the ESI source, whereas an in-source fragmentation technique allows the generation of smaller complexes, $x = 1−5$. Analysis of the CID data for both primary and secondary water loss is achieved using an empirical threshold model incorporating RRKM theory. This provides 0 K BDEs, which can be converted to 298 K BDEs using theoretically determined molecular parameters. Reasonable agreement between the primary and secondary BDEs is obtained, with the latter being systematically higher and the former being more reliable. BDEs for the $x = 1−3$ complexes are measured here for the first time. For the larger complexes, $x = 4−8$, the present primary TCID experimental values compare very well to those measured previously using BIRD[7] and fairly well with HPMS[3,5,6] results with differences similar to those found with other hydrated alkaline earth metal dications.[17−20]

Quantum chemical calculations were used to predict the GSs for the $Ba^{2+}(H_2O)_x$ complexes. All levels of theory agree on the GSs for $x = 1−6$, which match those previously calculated in the literature.[9−11] Different theoretical approaches yield different predicted geometries when secondary shells may begin to form for $x = 7$ and 8. B3LYP and B3P86 approaches suggest inner shells of six water ligands, whereas MP2 and M06 approaches indicate that seven and eight water ligands in the inner shell are competitive. Trends in the experimental bond energies are suggestive of CN = 6 for the inner shell of the $Ba^{2+}(H_2O)_x$ complexes; however, the ionic radius of Ba^{2+} is sufficiently large that water molecules bound directly to the Ba^{2+} atom and those bound in a second shell have similar BDEs. Furthermore, infrared photodissociation spectra from Williams and co-workers indicate appreciable populations of a (7,0) structure for $Ba^{2+}(H_2O)_7$ along with contributions from (6,1).[8] Overall, the inner shell CN for Ba^{2+} at 298 K is likely to include six, seven, and possibly eight water molecules.

The only reaction pathway observed for all $Ba^{2+}(H_2O)_x$ complexes activated by a collision with Xe is sequential water loss, although a very small amount of charge separation to $BaOH^+$ is witnessed from $Ba^{2+}(H_2O)_3$ under specific source conditions. This is unique compared to the hydrated alkaline earth metal dications previously studied in our laboratory,[17,19,20] where charge separation was observed at critical sizes of $x_c = 3$ (possibly 4) for Mg^{2+} and $x_c = 2$ for Ca^{2+} and Sr^{2+}. For complexes larger than x_c, the energy barrier required for water loss declines, whereas the Coulombic barrier stays relatively constant, such that the entropically disfavored charge separation channel is not observed. Quantum chemical calculations performed here and in the literature[11,16] show

DOI: 10.1021/acs.jpca.5b01087
J. Phys. Chem. A 2015, 119, 3800−3815

that the water loss pathway is lower in energy than the charge separation pathway for $Ba^{2+}(H_2O)_2$, consistent with the failure to observe this reaction. In contrast, at B3LYP and B3P86 levels of theory, we find that dissociation of $Ba^{2+}(H_2O)_3$ to $BaOH^+ + H_5O_2^+$ is energetically competitive with water loss, whereas MP2 and M06 results parallel literature calculations that again favor the water loss pathway.[16] The B3LYP and B3P86 results are consistent with the observation of a small $BaOH^+$ product cross section when the intensity of the $Ba^{2+}(H_2O)_3$ reactant is optimized.

■ ASSOCIATED CONTENT

Supporting Information

Additional tables including single-point energies for H_2O loss from $Ba^{2+}(H_2O)_x$, where $x = 1-8$, at four levels of theory using five different basis sets; a table of relative energies of low-lying conformers with and without dispersion corrections for $x = 7$ and 8; table of Ba−O bond distances for $x = 1-8$ calculated at several levels of theory; table showing the conversion between 0 K hydration energies and enthalpies and free energies at 298 K; table for modeling of our experimental data with vibrational frequencies of excited isomers; figures illustrating cross sections, primary channel modeling, and sequential modeling for $x = 1-8$; and a diagram showing the reaction coordinate for dissociation of $Ba^{2+}(H_2O)_2$. This material is available free of charge via the Internet at http://pubs.acs.org.

■ AUTHOR INFORMATION

Corresponding Author

*E-mail: armentrout@chem.utah.edu.

Present Addresses

[†]D.R.C.: Precision Diagnostics, LLC, 1070 East 86th Street, Suite 72F, Indianapolis, IN 46240.

[‡]T.E.H.: Air Force Technical Applications Center, Patrick Air Force Base, FL 32925.

Notes

The authors declare no competing financial interest.

■ ACKNOWLEDGMENTS

Funding for this work was provided by the National Science Foundation under Grant CHE-1359769. In addition, we thank the Center for High Performance Computing (CHPC) at the University of Utah for the generous allocation of computing time.

■ REFERENCES

(1) Basic Information about Barium in Drinking Water. Agency for Toxic Substances and Disease Registry, 2009. http://water.epa.gov/drink/contaminants/basicinformation/barium.cfm (accessed September 17, 2014).

(2) Toxicological Profile for Barium and Barium Compounds. Public Health Service, Agency for Toxic Substances and Disease Registry, 2005. http://www.atsdr.cdc.gov/toxprofiles/tp24.pdf (accessed September 17, 2014).

(3) Jayaweera, P.; Blades, A. T.; Ikonomou, M. G.; Kebarle, P. Production and Study in the Gas Phase of Multiply Charged Solvated or Coordinated Metal Ions. *J. Am. Chem. Soc.* **1990**, *112*, 2452−2454.

(4) Blades, A. T.; Jayaweera, P.; Ikonomou, M. G.; Kebarle, P. Ion−Molecule Clusters Involving Doubly Charged Metal Ions (M^{2+}). *Int. J. Mass Spectrom. Ion Processes* **1990**, *102*, 251−267.

(5) Blades, A. T.; Jayaweera, P.; Ikonomou, M. G.; Kebarle, P. Studies of Alkaline Earth and Transition Metal M^{+2} Gas Phase Ion Chemistry. *J. Chem. Phys.* **1990**, *92*, 5900−5906.

(6) Peschke, M.; Blades, A. T.; Kebarle, P. Hydration Energies and Entropies for Mg^{2+}, Ca^{2+}, Sr^{2+}, and Ba^{2+} from Gas-Phase Ion−Water Molecule Equilibria Determinations. *J. Phys. Chem. A* **1998**, *102*, 9978−9985.

(7) Rodriguez-Cruz, S. E.; Jockusch, R. A.; Williams, E. R. Hydration Energies and Structures of Alkaline Earth Metal Ions, $M^{2+}(H_2O)_n$, $n = 5-7$, M = Mg, Ca, Sr, and Ba. *J. Am. Chem. Soc.* **1999**, *121*, 8898−8906.

(8) Bush, M. F.; O'Brien, J. T.; Prell, J. S.; Wu, C.-C.; Saykally, R. J.; Williams, E. R. Hydration of Alkaline Earth Metal Dications: Effects of Metal Ion Size Determined Using Infrared Action Spectroscopy. *J. Am. Chem. Soc.* **2009**, *131*, 13270−13277.

(9) Kaupp, M.; Schleyer, P. v. R.; Stoll, H.; Preuss, H. Pseudopotential Approaches to Ca, Sr, and Ba Hydrides. Why are Some Alkaline Earth MX_2 Compounds Bent? *J. Chem. Phys.* **1991**, *94*, 1360−1366.

(10) Kaupp, M.; Schleyer, P. v. R. Do Low-Coordinated Group 1−3 Cations $M^{n+}L_m$ ($M^{n+} = K^+$, Rb^+, Cs^+, Ca^+, Sr^{2+}, Ba^{2+}, Sc^{3+}, Y^{3+}, La^{3+}; L= NH_3, H_2O, HF; $m = 1-3$) with a Formal Noble Gas Electron Configuration Favor Regular or "Abnormal" Shapes? *J. Phys. Chem.* **1992**, *96*, 7316−7323.

(11) Glendening, E. D.; Feller, D. Dication−Water Interactions: $M^{2+}(H_2O)_n$ Clusters for Alkaline Earth Metals M = Mg, Ca, Sr, Ba, and Ra. *J. Phys. Chem.* **1996**, *100*, 4790−4797.

(12) Cao, Y.-L.; Wang, Y.-S. Geometry Optimization of $Ba^{2+}(H_2O)_n$ Clusters Using a Fast Hybrid Global Optimization Algorithm. *J. Chin. Chem. Soc. (Taipei, Taiwan)* **2004**, *51*, 689−695.

(13) Beyer, M.; Williams, E. R.; Bondybey, V. E. Unimolecular Reactions of Dihydrated Alkaline Earth Metal Dications $M^{2+}(H_2O)_2$, M = Be, Mg, Ca, Sr, and Ba: Salt-Bridge Mechanism in the Proton-Transfer Reaction $M^{2+}(H_2O)_2 \rightarrow MOH^+ + H_3O^+$. *J. Am. Chem. Soc.* **1999**, *121*, 1565−1573.

(14) Becke, A. D. Density-functional Thermochemistry. III. The Role of Exact Exchange. *J. Chem. Phys.* **1993**, *98*, 5648−5652.

(15) Lee, C.; Yang, W.; Parr, R. G. Development of the Colle-Salvetti Correlation-Energy Formula into a Functional of the Electron Density. *Phys. Rev. B: Condens. Matter Mater. Phys.* **1988**, *37*, 785−789.

(16) Miliordos, E.; Xantheas, S. S. Unimolecular and hydrolysis channels for the detachment of water from microsolvated alkaline earth dication (Mg^{2+}, Ca^{2+}, Sr^{2+}, Ba^{2+}) clusters. *Theor. Chem. Acc.* **2014**, *133*, 1−12.

(17) Carl, D. R.; Armentrout, P. B. Threshold Collision-Induced Dissociation of Hydrated Magnesium: Experimental and Theoretical Investigation of the Binding Energies for $Mg^{2+}(H_2O)_x$ complexes ($x = 2-10$). *ChemPhysChem* **2013**, *14*, 681−697.

(18) Carl, D. R.; Moision, R. M.; Armentrout, P. B. Binding Energies for the Inner Hydration Shells of Ca^{2+}: An Experimental and Theoretical Investigation of $Ca^{2+}(H_2O)_x$ Complexes ($x = 5 - 9$). *Int. J. Mass Spectrom.* **2007**, *265*, 308−325.

(19) Carl, D. R.; Armentrout, P. B. Experimental Investigation of the Complete Inner Shell Hydration Energies of Ca^{2+}: Threshold Collision-Induced Dissociation of $Ca^{2+}(H_2O)_x$ Complexes ($x = 2 - 8$). *J. Phys. Chem. A* **2012**, *116*, 3802−3815.

(20) Carl, D. R.; Chatterjee, B. K.; Armentrout, P. B. Threshold Collision-Induced Dissociation of $Sr^{2+}(H_2O)_x$ Complexes ($x = 1 - 6$): An Experimental and Theoretical Investigation of the Complete Inner Shell Hydration Energies of Sr^{2+}. *J. Chem. Phys.* **2010**, *132*, 044303.

(21) Cooper, T. E.; Carl, D. R.; Armentrout, P. B. Hydration Energies of Zinc (II): Threshold Collision-Induced Dissociation Experiments and Theoretical Studies. *J. Phys. Chem. A* **2009**, *113*, 13727−13741.

(22) Cooper, T. E.; Armentrout, P. B. An Experimental and Theoretical Investigation of the Charge Separation Energies of Hydrated Zinc (II): Redefinition of the Critical Size. *J. Phys. Chem. A* **2009**, *113*, 13742−13751.

(23) Cooper, T. E.; Armentrout, P. B. Threshold Collision-Induced Dissociation of Hydrated Cadmium (II): Experimental and Theoretical Investigation of the Binding Energies for $Cd^{2+}(H_2O)_n$ Complexes ($n = 4 - 11$). *Chem. Phys. Lett.* **2010**, *486*, 1−6.

DOI: 10.1021/acs.jpca.5b01087
J. Phys. Chem. A 2015, 119, 3800−3815

(24) Cooper, T. E.; Armentrout, P. B. Sequential Bond Energies and Barrier Heights for the Water Loss and Charge Separation Dissociation Pathways of $Cd^{2+}(H_2O)_n$, n = 3−11. *J. Chem. Phys.* **2011**, *134*, 114308.
(25) Hofstetter, T. E.; Armentrout, P. B. Threshold Collision-Induced Dissociation and Theoretical Studies of Hydrated Fe(II): Binding Energies and Coulombic Barrier Heights. *J. Phys. Chem. A* **2013**, *117*, 1110−1123.
(26) Sweeney, A. F.; Armentrout, P. B. Guided Ion Beam Studies of the Collision-Induced Dissociation of $CuOH^+(H_2O)_n$ (n = 1−4): Comprehensive Thermodynamic Data for Copper Ion Hydration. *J. Phys. Chem. A* **2014**, *118*, 10210−10222.
(27) Carl, D. R.; Moision, R. M.; Armentrout, P. B. In-Source Fragmentation Technique for the Production of Thermalized Ions. *J. Am. Soc. Mass Spectrom.* **2009**, *20*, 2312−2317.
(28) Moision, R. M.; Armentrout, P. B. An Electrospray Source for Thermochemical Investigation with the Guided Ion Beam Mass Spectrometer. *J. Am. Soc. Mass Spectrom.* **2007**, *18*, 1124−1134.
(29) Shvartsburg, A. A.; Siu, K. W. M. Is There a Minimum Size for Aqueous Doubly Charged Metal Cations? *J. Am. Chem. Soc.* **2001**, *123*, 10071−10075.
(30) Bush, M. F.; Saykally, R. J.; Williams, E. R. Reactivity and Infrared Spectroscopy of Gaseous Hydrated Trivalent Metal Ions. *J. Am. Chem. Soc.* **2008**, *130*, 9122−9128.
(31) Feil, S.; Koyanagi, G. K.; Bohme, D. K. Heavy Water Reactions with Alkaline-Earth Metal Dications in the Gas Phase: Kinetics at Room Temperature. *Int. J. Mass Spectrom.* **2009**, *280*, 38−41.
(32) Ervin, K. M.; Armentrout, P. B. Translational Energy Dependence of $Ar^+ + XY \rightarrow ArX^+ + Y$ (XY = H_2, D_2, HD) from Thermal to 30 eV c.m. *J. Chem. Phys.* **1985**, *83*, 166−189.
(33) Muntean, F.; Armentrout, P. B. Guided Ion Beam Study of Collision-Induced Dissociation Dynamics: Integral and Differental Cross Sections. *J. Chem. Phys.* **2001**, *115*, 1213−1228.
(34) Whitehouse, C. M.; Dreyer, R. N.; Yamashita, M.; Fenn, J. B. Electrospray Interface for Liquid Chromatographs and Mass Spectrometers. *Anal. Chem.* **1985**, *57*, 675−679.
(35) Shaffer, S. A.; Prior, D. C.; Anderson, G. A.; Udseth, H. R.; Smith, R. D. An Ion Funnel Interface for Improved Ion Focusing and Sensitivity Using Electrospray Ionization Mass Spectrometry. *Anal. Chem.* **1998**, *70*, 4111−4119.
(36) Kim, T.; Tang, K.; Udseth, H. R.; Smith, R. D. A Multicapillary Inlet Jet Disruption Electrodynamic Ion Funnel Interface for Improved Sensitivity Using Atmospheric Pressure Ion Sources. *Anal. Chem.* **2001**, *73*, 4162−4170.
(37) Teloy, E.; Gerlich, D. Integral Cross Sections for Ion−Molecule Reactions. 1. The Guided Beam Technique. *Chem. Phys.* **1974**, *4*, 417−427.
(38) Gerlich, D. Inhomogeneous rf Fields: A Versatile Tool for the Study of Processes with Slow Ions. *Adv. Chem. Phys.* **1992**, *82*, 1−176.
(39) Aristov, N.; Armentrout, P. B. Collision-Induced Dissociation of Vanadium Monoxide Ion. *J. Phys. Chem.* **1986**, *90*, 5135−5140.
(40) Dalleska, N. F.; Honma, K.; Sunderlin, L. S.; Armentrout, P. B. Solvation of Transition Metal Ions by Water. Sequential Binding Energies of $M^+(H_2O)_x$ (x = 1−4) for M = Ti to Cu Determined by Collision-Induced Dissociation. *J. Am. Chem. Soc.* **1994**, *116*, 3519−3528.
(41) Daly, N. R. Scintillation Type Mass Spectrometer Ion Detector. *Rev. Sci. Instrum.* **1960**, *31*, 264−267.
(42) Hales, D. A.; Lian, L.; Armentrout, P. B. Collision-Induced Dissociation of Nb_n^+ (n = 2−11): Bond Energies and Dissociation Pathways. *Int. J. Mass Spectrom. Ion Processes* **1990**, *102*, 269−301.
(43) Holbrook, K. A.; Pilling, M. J.; Robertson, S. H. *Unimolecular Reactions*, 2nd ed.; Wiley: New York, 1996.
(44) Gilbert, R. G.; Smith, S. C. *Theory of Unimolecular and Recombination Reactions*; Blackwell Scientific: London, 1990.
(45) Truhlar, D. G.; Garrett, B. C.; Klippenstein, S. J. Current Status of Transition-State Theory. *J. Phys. Chem.* **1996**, *100*, 12771−12800.
(46) Rodgers, M. T.; Ervin, K. M.; Armentrout, P. B. Statistical Modeling of Collision-Induced Dissociation Thresholds. *J. Chem. Phys.* **1997**, *106*, 4499−4508.
(47) Beyer, T. S.; Swinehart, D. F. Number of Multiply-Restricted Partitions. *Commun. ACM* **1973**, *16*, 379.
(48) Stein, S. E.; Rabinovich, B. S. On the Use of Exact State Counting Methods in RRKM Rate Calculations. *Chem. Phys. Lett.* **1977**, *49*, 183−188.
(49) Stein, S. E.; Rabinovitch, B. S. Accurate Evaluation of Internal Energy Level Sums and Densities Including Anharmonic Oscillators and Hindered Rotors. *J. Chem. Phys.* **1973**, *58*, 2438−2445.
(50) Armentrout, P. B. Statistical Modeling of Sequential Collision-Induced Dissociation. *J. Chem. Phys.* **2007**, *126*, 234302.
(51) Armentrout, P. B.; Simons, J. Understanding Heterolytic Bond Cleavage. *J. Am. Chem. Soc.* **1992**, *114*, 8627−8633.
(52) Waage, E. V.; Rabinovitch, B. S. Centrifugal Effects in Reaction Rate Theory. *Chem. Rev. (Washington, DC, U.S.)* **1970**, *70*, 377−387.
(53) Frisch, M. J.; Trucks, G. W.; Schlegel, H. B.; Scuseria, G. E.; Robb, M. A.; Cheeseman, J. R.; Scalmani, G.; Barone, V.; Mennucci, B.; Petersson, G. A., et al. *Gaussian 09*, revision A.02; Gaussian Inc.: Pittsburgh, PA, 2009.
(54) Weigend, F.; Ahlrichs, R. Def2-SVP Basis Sets. *Phys. Chem. Chem. Phys.* **2005**, *7*, 3297−3305.
(55) Hay, P. J.; Wadt, W. R. Ab Initio Effective Core Potentials for Molecular Calculations. Potentials for K to Au Including the Outermost Core Orbitals. *J. Chem. Phys.* **1985**, *82*, 299−310.
(56) Heaton, A. L.; Bowman, V. N.; Oomens, J.; Steill, J. D.; Armentrout, P. B. Infrared Multiple Photon Dissociation Spectroscopy of Cationized Asparagine: Effects of Metal Cation Size on Gas-Phase Conformation. *J. Phys. Chem. A* **2009**, *113*, 5519−5530.
(57) Bauschlicher, C. W.; Partridge, H. A Modification of the Gaussian-2 Approach Using Density Functional Theory. *J. Chem. Phys.* **1995**, *103*, 1788−1791.
(58) Zhao, Y.; Truhlar, D. G. The M06 Suite of Density Functionals for Main Group Thermochemistry, Thermochemical Kinetics, Noncovalent Interactions, Excited States, and Transition Elements: Two New Functionals and Systematic Testing of Four M06-Class Functionals and 12 Other Functionals. *Theor. Chem. Acc.* **2008**, *120*, 215−241.
(59) Boys, S. F.; Bernardi, R. The Calculation of Small Molecular Interactions by the Differences of Separate Total Energies. Some Procedures with Reduced Errors. *Mol. Phys.* **1970**, *19*, 553−566.
(60) van Duijneveldt, F. B.; van Duijneveldt-van de Rijdt, J. G. C. M.; van Lenthe, J. H. State of the Art in Counterpoise Theory. *Chem. Rev. (Washington, DC, U.S.)* **1994**, *94*, 1873−1885.
(61) Lim, I. S.; Stoll, H.; Schwerdtfeger, P. Relativistic Small-Core Energy-Consistent Pseudopotentials for the Alkaline-Earth Elements from Ca to Ra. *J. Chem. Phys.* **2006**, *124*, 034107.
(62) Grimme, S.; Ehrlich, S.; Goerigk, L. Effect of the Damping Function in Dispersion Corrected Density Functional Theory. *J. Comput. Chem.* **2011**, *32*, 1456−1465.
(63) Goerigk, L.; Grimme, S. Efficient and Accurate Double-Hybrid-Meta-GGA Density Functionals—Evaluation with the Extended GMTKN30 Database for General Main Group Thermochemistry, Kinetics, and Noncovalent Interactions. *J. Chem. Theory Comput.* **2011**, *7*, 291−309.
(64) Cooper, T. E.; O'Brien, J. T.; Williams, E. R.; Armentrout, P. B. Zn^{2+} Has a Primary Hydration Sphere of Five: IR Action Spectroscopy and Theoretical Studies of Hydrated Zn^{2+} Complexes. *J. Phys. Chem. A* **2010**, *114*, 12646−12655.
(65) Wilson, R. G.; Brewer, G. R. *Ion Beams with Applications to Ion Implantation*; Wiley: New York, 1973.
(66) Rodgers, M. T.; Armentrout, P. B. A Critical Evaluation of the Experimental and Theoretical Determination of Lithium Cation Affinities. *Int. J. Mass Spectrom.* **2007**, *267*, 167−182.

DOI: 10.1021/acs.jpca.5b01087
J. Phys. Chem. A 2015, 119, 3800−3815